12-2006

Neutron Diffraction Study of Heavy Water Intercalation in Superconducting Deuterated Sodium Cobaltate $Na_{0.35}CoO_21.4D_2O$

Cinzia Metallo
University of Tennessee - Knoxville

To the Graduate Council:

I am submitting herewith a thesis written by Cinzia Metallo entitled "Neutron Diffraction Study of Heavy Water Intercalation in Superconducting Deuterated Sodium Cobaltate $Na_{0.35}CoO_2 1.4D_2O$." I have examined the final electronic copy of this thesis for form and content and recommend that it be accepted in partial fulfillment of the requirements for the degree of Master of Science, with a major in Physics.

Takeshi Egami, Major Professor

We have read this thesis and recommend its acceptance:

Elbio R. A. Dagotto, James R. Thompson

Accepted for the Council:
Carolyn R. Hodges

Vice Provost and Dean of the Graduate School

(Original signatures are on file with official student records.)

To the Graduate Council:
I am submitting herewith a thesis written by Cinzia Metallo entitled "Neutron Diffraction Study of Heavy Water Intercalation in Superconducting Deuterated Sodium Cobaltate $Na_{0.35}CoO_2 1.4D_2O$". I have examined the final electronic copy of this thesis for form and content and recommend that it be accepted in partial fulfillment of the requirements for the degree of Master of Science, with a major in Physics.

Takeshi Egami
Major Professor

We have read this thesis
and recommend its acceptance:

Elbio R. A. Dagotto

James R. Thompson

Accepted for the Council:

Linda Painter
Interim Dean of Graduate Studies

(Original signatures are on file with official student records.)

NEUTRON DIFFRACTION STUDY OF HEAVY WATER INTERCALATION IN SUPERCONDUCTING DEUTERATED SODIUM COBALTATE $Na_{0.35}\ C_OO_2\ 1.4D_2O$

A Thesis Presented for
the Master of Science
Degree

The University of Tennessee, Knoxville

Cinzia Metallo

December 2006

Acknowledgments

Coming to the States for my graduate studies has revealed itself to be, at times more rewarding, and at times more difficult than I had envisioned. I had a vague idea of what doing research really meant and I had no idea if the American way of life would have suited me. The final result of this experience is rather positive.

In these past two years I had the chance to get to know people that will permanently be "stored" in the sector of my mind devoted to the special people I met. First of all, my advisor Takeshi Egami. He showed me that fun and physics are not mutually exclusive. His constant enthusiasm was enlightening in the many "black-out periods" I had. He has been a source of inspiration and precious advice in both professional and personal matters. He gave me the possibility to travel, both nationally and internationally, to present my work. I will always be thankful to him for his help and support.

A thanks goes out also to my teammates, Ferenc and Zsolt. Their invaluable friendship, their sarcasm, and the endless chatting we had about physics and "stuff" helped me through these years. I will miss our trips to Starbucks!

A thank you to my parents may seem rhetorical here, but I could not have accomplished all this without their support, which always arrives strong even if from the other side of the ocean.

Thank you to the group of David Mandrus for providing the samples that made this work possible. To Thomas Proffen, for his help with the programs PDFgetN and PDFFIT. To Jae-Ho, who is the one that actually collected the data I analyzed and who shared with me his past experience with cobaltates.

Finally, thank you to Allen, who (more or less!) patiently reviewed the English part of this thesis. If you, dear reader, will happen to find any English grammar mistakes, you know who is to blame! I take my share of responsibility for the physics part, of course!

Abstract

Neutron diffraction study of heavy water intercalation in superconducting deuterated sodium cobaltate $Na_{0.35}CoO_2 1.4D_2O$

Cinzia Metallo

Takeshi Egami

When Na-deficient Na_xCoO_2 is intercalated with water[1] or heavy water[2], it becomes a superconductor. The maximum critical temperature of 4.5 K is found for the composition $Na_xCoO_2yD_2O$ (x= 0.3 and y=1.4). In spite of its low transition temperature, several similarities with high temperature superconducting cuprates have raised interest in this compound. Nevertheless, up to now, a clear understanding of the role of water has not been achieved.

Since superconductivity appears only when water is inserted in the parent compound, the goal of this research work was to understand what kind of effect water intercalation has in terms of electron conduction and superconductivity. Neutron scattering played a crucial role in this study because of its ability to determine the accurate positions of light elements such as hydrogen or deuterium.

We have focused our attention on the intra-molecular range of D_2O, studying the structural changes that take place within the (heavy) water molecules themselves. In order to do this the distance correlations D-D, D-O, and O-O have been studied.

Powder neutron diffraction data of the deuterated sodium cobaltate have been analyzed using the Pair Density Function (PDF) technique, which gives information about the local structure of the water molecules. The peaks of the PDF of the neutron diffraction data, in fact, give directly in real space the distances between pair of atoms, in this case the distances D-D, D-O, and O-O. If a peak shifts to a lower (or higher) value of *r* (Å) it means that the bond between that particular pair of atoms has become shorter (or

longer). In this way it was possible to determine any change in the geometry of the water molecules.

The results obtained show that the D-D distance and the D-O-D angle in $Na_{0.35}CoO_2 1.4D_2O$ are significantly different from those of ordinary water (D_2O). Two coexisting distributions of possible D-O-D bond angles are observed. We speculate that the altered geometry of the intercalated water molecules is due to a modification of the dynamics of the hydrogen bond. In this case, water may be embedded in an electronically active environment and indirectly participate in electronic conduction.

Table of Contents

List of Tables

List of Figures

Chapter 1

Introduction

In 2003, a new superconductor was discovered in the hydrated form of sodium cobalt oxide.[1] What makes this compound extremely peculiar is that superconductivity is achieved by intercalating the Na-deficient compound Na_xCoO_2 with water.

In this chapter, the motivations that induced us to study the deuterated sodium cobaltate $Na_{0.3}CoO_2 1.4D_2O$ and the main purpose of this dissertation are presented. At the end of the chapter, the organization of the rest of this thesis is explained in detail.

1.1 Background of the research

Sodium cobalt oxide Na_xCoO_2 was discovered about 30 years ago. The relatively large thermoelectric power, combined with a low resistivity, has made it the object of an intense investigation due to its potentially promising applications as a thermoelectric material.

In 2003, the discovery of superconductivity in the hydrated[1,3] (or deuterated[2]) form of the sodium cobalt oxide ($Na_xCoO_2yH_2O$) has renewed research interest in this oxide system. The superconducting phase $Na_xCoO_2yH_2O$ is obtained from the parent compound Na_xCoO_2 through oxidative de-intercalation of Na^+ and subsequent intercalation of water in between each pair of adjacent CoO_2 layers.

The study of hydrated sodium cobalt oxide is particularly interesting, despite its low transition temperature (T_C~4.5 K), because of the existence of several analogies with the more studied high temperature superconducting cuprates (*paragraph 1.2.3*). Understanding of the mechanism that gives rise to superconductivity in this compound may help to uncover the superconducting mechanism in high temperature

superconductors. The similarities with cuprate superconductors are mainly: (1) both have a layered crystal structure with the charge mainly in the plane composed of magnetic ions; (2) T_C strongly depends on doping. Electronically active planes (CuO_2 layers in cuprates, CoO_2 layers in cobaltates) alternate with non superconducting planes (Na layers) that act as space separators and as charge reservoirs. In reality, the CoO_2 plane in cobaltates is a layer of edge sharing CoO_6 octaedra, while CuO_2 layers in cuprates have Cu with square-planar coordination with a O-Cu-O bond angle of about 180º. Furthermore, the optimal T_C occurs in a narrow range of Na concentrations and decreases in both under and over doped materials, in analogy with the phase diagram of cuprates which displays a doping-dependent behavior.

The dependence of T_C on the water concentration (y) is a central issue. As the water content approaches the value y~1.4 (where the superconducting phase appears), water molecules separate from the Na layer and go to form additional H_2O layers between the Na and CoO_2 layers. As a consequence, the spatial separation between the CoO_2 layers becomes bigger and the c-axis lattice parameter increases from 11.2 Å (y=0) to 19.6 Å (y=1.4).[4] As of today, there is no agreement on the exact spatial arrangement of the water molecules between the Na and CoO_2 layers.[5]

Despite the fact that it is generally believed that the effect of the hydrogenation is only to enhance the two-dimensionality of the structure and increase spin fluctuations, a clear understanding of the role of water has not yet been achieved.

In this thesis, the problem of understanding the effect of water intercalation in sodium cobaltate was approached by asking the following question: what if the role of water is not only to enhance the two-dimensionality but also to actively help to set the superconducting mechanism? The technique chosen to answer this question was neutron scattering because of its ability to detect light atoms such as H. In order to avoid the disturbing background due to inelastic scattering from H, however, we have chosen to deuterate our sample instead of hydrating it. The results of this investigation are chronicled in these pages.

1.2 Organization of the thesis

In this thesis, I will report on experiments we have done using neutron diffraction to elucidate what role water may play in triggering the superconducting state in the cobalt oxide compound $Na_{0.35}CoO_2 1.4D_2O$.

In chapter two, some basic features of conventional and high temperature superconductors will be briefly reviewed. A parallel between cuprate superconductors and cobaltate superconductors will be also made.

In chapter three, the basic theory of neutron scattering and the technique used to analyze our neutron diffraction data, the Pair Distribution Function (PDF) technique, will be illustrated.

In chapter four, the sample preparation and the properties of the compounds studied ($Na_{0.7}CoO_2$, $Na_{0.35}CoO_2 1.4D_2O$, and D_2O) will be described.

Finally in chapter five, the experimental analysis will be introduced, and the possible implications of our results will be discussed.

Chapter 2

Basic theory of superconductivity

Since the compound studied is a superconductor, in this chapter a brief review of some basic concepts of superconductivity is presented.

2.1 Properties of a superconductor

A superconductor is a material characterized by the following two properties:

(a) No resistivity ($\rho=0$) for all temperatures $T<T_C$, where T_C is the critical temperature (*figure 2.1a*);

(b) No magnetic induction ($B=0$) inside the superconductor (Meissner effect) for small applied magnetic fields (*figure 2.1b*).

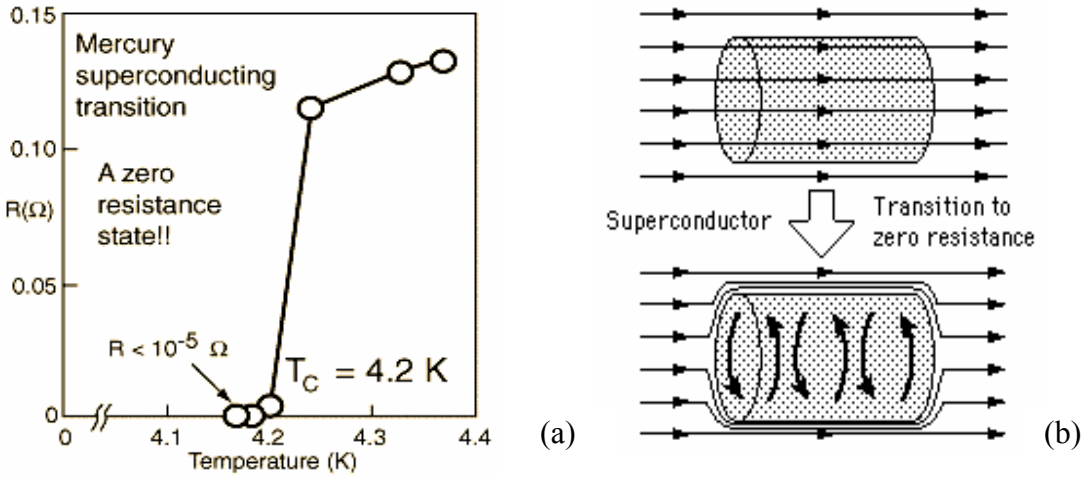

Figure 2.1: Properties of a superconductor: (a) below the critical temperature T_C, the electrical resistivity goes to zero; (b) below the critical applied magnetic field H_C the magnetic flux is expelled (Meissner effect).

The phenomenon of superconductivity was first discovered by H. K. Onnes[6] in 1911 while investigating the electrical properties of metals at extremely cold temperatures. When he passed a current through a very pure mercury wire and measured its resistance at steadily decreasing temperatures, he surprisingly found that the resistance suddenly vanished at 4.2 K. In the years to follow many other metallic elements were discovered to superconduct at very low temperatures (for example lead has T_C= 7.2 K and Nb has T_C=9.2 K)

In 1933 Meissner and Ochsenfeld[7] discovered the second surprising property of the superconducting state: perfect diamagnetism. Below the critical value H_C of an applied magnetic field, the magnetic flux is expelled from the interior of the superconductor. A superconductor does not allow a magnetic field to penetrate its interior. If the applied magnetic field is strong enough, it penetrates the interior of the metal and the metal loses its superconductivity. This phenomenon is called the Meissner effect and it is the reason why a magnet can levitate above a superconductor.

Superconducting materials that completely expel the magnetic flux below a certain critical field H_C are called type I superconductors. Superconductors that have two critical fields H_{C1} and H_{C2} are called type II superconductors. While the flux is completely expelled up to H_{C1}, it partially penetrates into the material between H_{C1} and H_{C2} in the form of microscopic filaments called vortices. Above H_{C2} the material returns to the normal state.

2.2 Conventional superconductors

Although superconductivity was discovered in 1911, it was not until 1957 that Bardeen, Cooper, and Schrieffer (Nobel Prize 1957) proposed a complete microscopic theory of the phenomenon, the so called BCS theory.[8]

The basic idea of BCS theory is that electrons (fermions) pair via phonon coupling and the pairs (bosons, called Cooper pairs) condense into a single coherent ground state which allows the electrons to move cooperatively through the crystal in a single coherent motion. The electrons that form each Cooper-pair have opposite spins and

momenta, so the net momentum p of the pair is zero. By the de Broglie relation ($\lambda = \frac{h}{p}$), the associated wave has infinite wavelength (in more realistic physical terms it means that it is of the order of the size of the sample). As a consequence, superconductivity is a quantum phenomenon on a macroscopic scale. In other words, the superconducting ground-state is essentially the condensation of the Cooper-pairs into a single macroscopic quantum state – a process analogous to Bose-Einstein condensation. In the normal state of a metal, the scattering of conduction electrons (by lattice vibrations, impurities, or lattice imperfections) contributes to resistivity. In the superconducting state, on the other hand, since there is no scattering of individual pairs of the coherent fluid, there is no resistivity. Once the collective, highly coordinated, state of coherent Cooper pairs is set into motion, its flow is without dissipation.

The fact that the 'glue' that pairs electrons is provided by lattice elastic waves (phonons) was shown experimentally by the isotope effect, according to which two different isotopes of the same metal exhibit different critical temperatures.[9,10] For some simple metals, the critical temperature T_C was found to vary as the inverse square root of the nuclear mass: $T_C \sim m^{-\frac{1}{2}}$. Since the phonon frequency varies as $\omega \sim \sqrt{\frac{k}{m}}$, the discovery of the isotope effect led to the conclusion that phonons are indeed involved in the pairing mechanism.

In conventional superconductors, the order parameter (OP) associated with this BCS ground-state typically has s-wave symmetry. The formation of Cooper-pairs opens a gap of width Δ in the density of electronic states at the Fermi level.[11, 12] The quantity Δ depends on temperature and it is referred to as the superconducting energy gap (or superconducting order parameter).

With the BCS theory, the problem of superconductivity was largely considered solved. Despite many efforts to find materials that could superconduct at higher temperatures, for decades the highest known transition temperature was of about 23 K (Nb_3Ge). A huge surprise, however, was yet to come.

2.3 The discovery of High-Temperature Superconductors

In 1986, Georg Bednorz and Alex Müller (IBM Zurich, Switzerland), discovered a new class of superconducting materials with transition temperatures much higher than the old record of 23 K. They were experimenting with a particular class of metal oxide ceramics called perovskites, when they found that ceramics of lanthanum, barium, copper, and oxygen ($La_{2-x}Ba_xCuO_4$) had a surprisingly high T_C of 30 K.[13] The once stagnant field of superconductivity research suddenly reopened. In 1987, the liquid nitrogen temperature barrier (77 K) was broken with the discovery of $YBa_2Cu_3O_{7-\delta}$, superconducting at 90 K;[14] now it became possible to use liquid nitrogen as a coolant, which is inexpensive compared to liquid helium.

Soon after 1987, compounds that superconduct at temperatures over 130 K were discovered. Because these materials superconduct at significantly higher temperatures than the class of conventional superconductors, they are referred to as High Temperature Superconductors (HTSCs). Also, since the common component in this new class of high temperature superconductors is a CuO_2 plane, these materials are referred to as the *cuprates*. The main steps in the history of the increase in T_C are shown in *figure 2.2*.

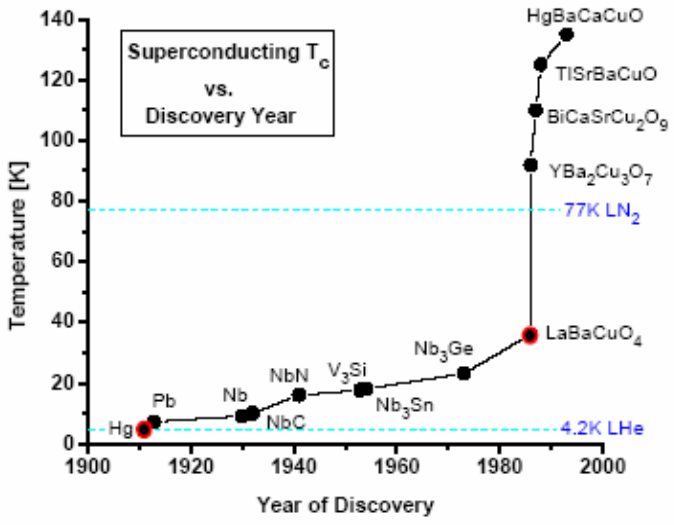

Figure 2.2: Advancement in the history of superconductivity. The two red points represent the Nobel Prizes of Kamerlingh-Onnes (1913) and Bednorz & Müller (1987).

2.4 Basic remarks on HTSCs

A detailed treatment of HTSCs is beyond the scope of this thesis. However, since similarities with cuprates are one of the reasons why interest in cobaltates has been so high, a few general remarks will be made.

The discovery of high-temperature superconductivity created a great deal of excitement. Nevertheless, up to now, no satisfactory explanation of the superconducting mechanism has been given.

High-temperature cuprate superconductors consist of layers of copper and oxygen, separated by metal atoms such as yttrium and barium (*figure 2.3c)*. Probably one of the most complicating factors is the existence of a new tunable parameter, the carrier concentration (doping). This additional parameter leads to a 3-dimensional phase diagram (*figure 2.3a*). The stoichiometric (undoped) parent compounds are antiferromagnetic Mott insulators, and it is not until charge carriers are added that these materials become superconducting. In other words, superconductivity is achieved by doping (usually with holes) and it is believed to originate in the CuO_2 planes.

In a similar fashion, a sodium cobaltate superconductor consists of layers of cobalt and oxygen separated by layers of sodium; water molecules are incorporated into the structure between these two planes[1] (*figure 2.3d*). As for HTSCs, there is a clear dependence of T_C on doping (*figure 2.3b*) and the electronically active planes are those containing the magnetic ions (Co). The main difference between the two structures is the geometry of such planes. The Cu atoms in the CuO_2 plane form a square lattice (*figure 2.3e*), while the Co atoms in the CoO_2 plane form a triangular lattice (*figure 2.3d*). The phase diagram of sodium cobaltate will be thoroughly discussed in *chapter 4*.

In HTSCs, as in the case of conventional superconductors, it is now generally agreed that there is a gap in the density of states. However, instead of the simple symmetric *s*-wave gap found in conventional superconductors, the gap is dx_2-y_2-wave.[15,16] In simple terms, the dx_2-y_2-wave gap means that electrons traveling different directions in the crystal feel a different pairing potential.

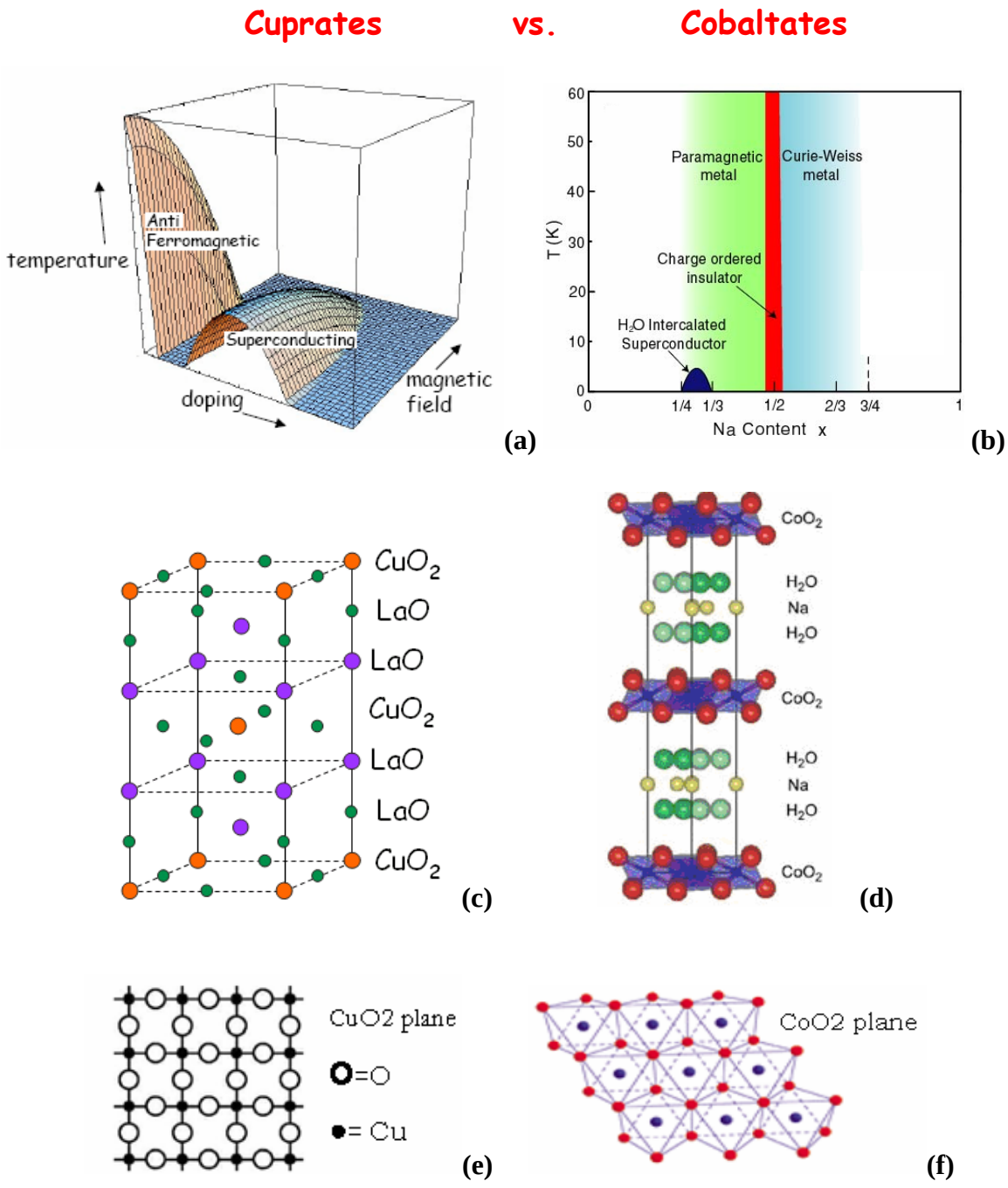

Figure 2.3: Similarities and differences between cuprates and cobaltates. **(a)** 3D phase diagram of HTSCs. **(b)** Proposed 2D phase diagram of cobaltates. In both cases superconductivity is achieved by varying the carrier concentration *x* (doping). **(c)** Layered structure of the high temperature superconductor $La_{2-x}Sr_xCuO_4$, taken as an example of the cuprate family. **(d)** Layered structure of $Na_xCoO_2yH_2O$. Electronically active planes are, respectively, **(e)** the square CuO_2 planes and **(f)** the triangular CoO_2 planes.

As it would be expected from the gap in the density of states, it is generally agreed that electrons are paired.[17] However, it is not generally agreed what causes the pairing. Some argue that electron pairing is caused by magnons or other magnetic consequences, but there are also strong arguments that pairing is indeed caused by phonons.[18]

Chapter 3

Experimental techniques

This thesis documents the use of neutron diffraction to investigate the effect of heavy water intercalation in superconducting deuterated sodium cobalt oxide $Na_{0.35}CoO_2 1.4D_2O$. Diffraction data were analyzed using the PDF technique, which gives information about local ordering in real space. This chapter introduces the fundamentals of both neutron scattering and the PDF technique.

3.1 Principal properties of neutrons

The neutron is a subatomic particle discovered by James Chadwick in 1932 (Nobel Prize, 1935). Since then, neutrons have found a variety of applications in different fields, from military applications to energy supply, from nuclear medicine to many areas of condensed matter physics.

Two main characteristics of neutrons are responsible for their unique scattering properties: they are uncharged, and they have a relatively large mass (m_n =1.6749 10^{-27} kg= ~1839 times the electron mass), which is nearly that of protons. The consequences of these properties of neutrons are of extreme importance:

(1) Energetic neutrons can be slowed down (moderated) by collision with atoms of similar mass (such as H or D) so that they can be led to have energies of the same order of magnitude as those of phonons (a neutron with wave vector k of a few $Å^{-1}$ has an energy of a few meV). Nevertheless, there are restrictions on the scattering vector Q for large energy transfer: excitations can be studied up to ~100 meV.

(2) Neutrons interact with matter only very weakly but penetrate deeply into the sample, better than charged particles; they can be used as non-destructive probes to measure bulk

properties of a variety of materials. Some elements strongly absorb neutrons and should be avoided (e.g. Cd, Gd, B).

(3) Neutrons interact directly with the atomic nuclei through a very short-range interaction (on the order of few Fermis, 1 fm=10^{-15} m).

(4) There is no systematic dependence of the penetration depth on the atomic number; neutrons can probe light atoms and make strong contrasts (i.e. H/D).

Neutrons also posses a magnetic moment and therefore represent an important tool in developing magnetic materials: they can be used to study microscopic magnetism, magnetic structure, and magnetic fluctuations (magnons).

Because of the low brilliance of neutron sources and the small scattering section of neutrons, long beam-times and relatively large samples are usually necessary. Furthermore, since neutron scattering requires a high intensity flux, continuous improvements of neutron sources are essential in order to achieve a higher resolution.

3.2 Basic theory of neutron scattering

In a neutron scattering experiment, the number of neutrons scattered by a sample is measured as a function of the wave-vector change (Q) and the energy change (ΔE) of the neutrons. A scattering event is based on the following two conservation laws for energy and momentum:[19]

$\hbar\vec{Q} = \hbar(\vec{K}_i - \vec{K}_f)$ *Momentum transfer*

$\hbar\omega = \Delta E = E_i - E_f = \frac{\hbar^2}{2m_n}(K_i^2 - K_f^2)$ *Energy transfer*

The subscript *f* refers to the outgoing beam, while the subscript *i* refers to the incoming beam. As a consequence, $\Delta E > 0$ denotes the excitation and $\Delta E < 0$ the de-excitation of the system. In a neutron scattering experiment, these conservation laws limit the accessible energy and momentum transfers.

Neutron scattering can be *elastic* or *inelastic*. In an elastic scattering event, the neutron is deflected but does not change its initial energy. In an inelastic scattering event,

the neutron either loses or gains energy. *Figure 3.1* shows the two cases through the well-known scattering triangles.

The intensity of the scattered neutrons (number of neutrons scattered per incident neutron) can be expressed as a function of the momentum transfer $\hbar\mathbf{Q}$ and the energy transfer $\Delta E = \hbar\omega$. This intensity $I(\mathbf{Q}, \Delta E)$ is proportional to the Fourier transform of a time-dependent pair correlation function $S(\mathbf{r},t)$, which gives the probability of finding two atoms at a certain distance r (Van Hove's formulation). Because of this correlation between the positions of the atoms, neutron scattering can be used to probe the structure of a material.[20]

Two types of scattering can occur: *coherent* and *incoherent* scattering. In the first case the scattered waves from all the nuclei have definite relative phases and can interfere; elastic coherent scattering (diffraction) gives information about the equilibrium structure, inelastic coherent scattering gives information about the relative motions of the atoms (lattice vibrations). In the case of incoherent scattering, the scattered waves have indeterminate relative phase and do not interfere; therefore, information about atomic diffusion can be gathered.

When a neutron passes through a sample, some of its energy may be transferred to the crystal to create lattice vibrations (neutron energy loss = phonon creation) with a characteristic frequency ω. If the crystal is already 'excited', on the other hand, a phonon can transfer its energy to the neutron (neutron energy gain = phonon annihilation). The two inelastic processes of phonon annihilation and phonon creation are related to each other by the principle of detailed balance:

$$S(-\vec{Q},-\omega) = \exp\left(\frac{-\hbar\omega}{K_B T}\right) S(\vec{Q},\omega)$$

In the above expression $S(\mathbf{Q},\omega)$ is the scattering function, K_B is the Boltzmann constant, T is the temperature, and ω is the frequency, which is assumed to be positive. Low temperature measurements are usually done with phonon creation.

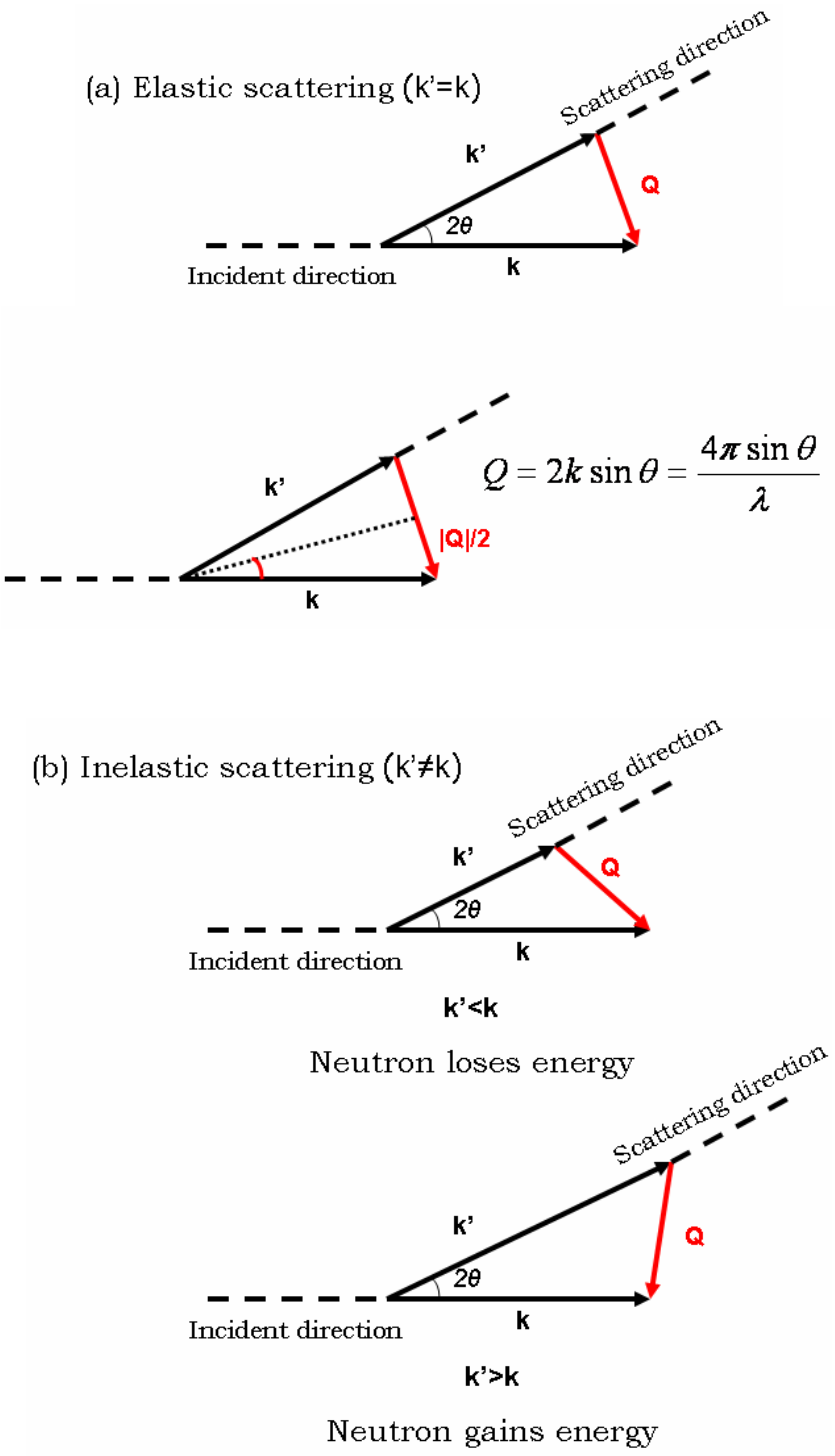

Figure 3.1: Scattering triangle for **(a)** elastic and **(b)** inelastic scattering. In the case of inelastic scattering, the exchange of energy and momentum between the incident beam and the sample causes the change of direction and magnitude of the neutrons.

An important quantity in any neutron scattering experiment is the scattering length *b*, which measures the strength of the neutron-nucleus interaction or, in other words, the scattering power of each scatterer. The real part of the scattering length is related to the scattering of neutrons; its imaginary part is related to the absorption of the neutron by a nucleus, but it is usually negligible. Since the spatial extent of the nuclear potential is virtually infinitesimal, *b* does not strongly depend on the scattering angle. The fact that different nuclear isotopes have different *b* is used in various isotopic-labeling techniques (D/H contrast variation, for example). The scattering length can assume negative values, like for H; when this happens, it means that there is a phase shift of π.

The scattering length *b* is related to the scattering cross section σ, which is the effective area made available to the incoming neutron. Looking at *figure 3.2*, we can define a differential cross section and a total cross section respectively as:[21]

$$\frac{d\sigma}{d\Omega} = \frac{\text{number of neutrons scattered per second into d}\Omega \text{ in the direction } (\theta, \phi)}{\Phi \, \text{d}\Omega}$$

$$\sigma_{TOT} = \frac{\text{number of neutrons scattered per second}}{\Phi}$$

In the above expressions, the total number of neutrons represents the number of neutrons scattered in all directions; dΩ is the solid angle subtended by the counter at the target; the direction (θ, ϕ) is the direction of the scattered neutrons in polar coordinates; Φ is the flux of incident neutrons. The expression of the total cross section includes a coherent and an incoherent part:

$$\sigma_{TOT} = \sigma_{coh} + \sigma_{incoh}$$

In elastic scattering, the coherent part contributes to the Bragg intensity, while the incoherent part contributes to the off-Bragg intensity. The total scattering cross section can also be written as:

$$\sigma_{TOT} = 4\pi\overline{|b|^2} = 4\pi|\bar{b}|^2 + 4\pi(\overline{|b|^2} - |\bar{b}|^2) = 4\pi b_{coh}^2 + 4\pi b_{incoh}^2 = \sigma_{coh} + \sigma_{incoh}$$

Table 3.1 shows the scattering length and cross section for different elements.

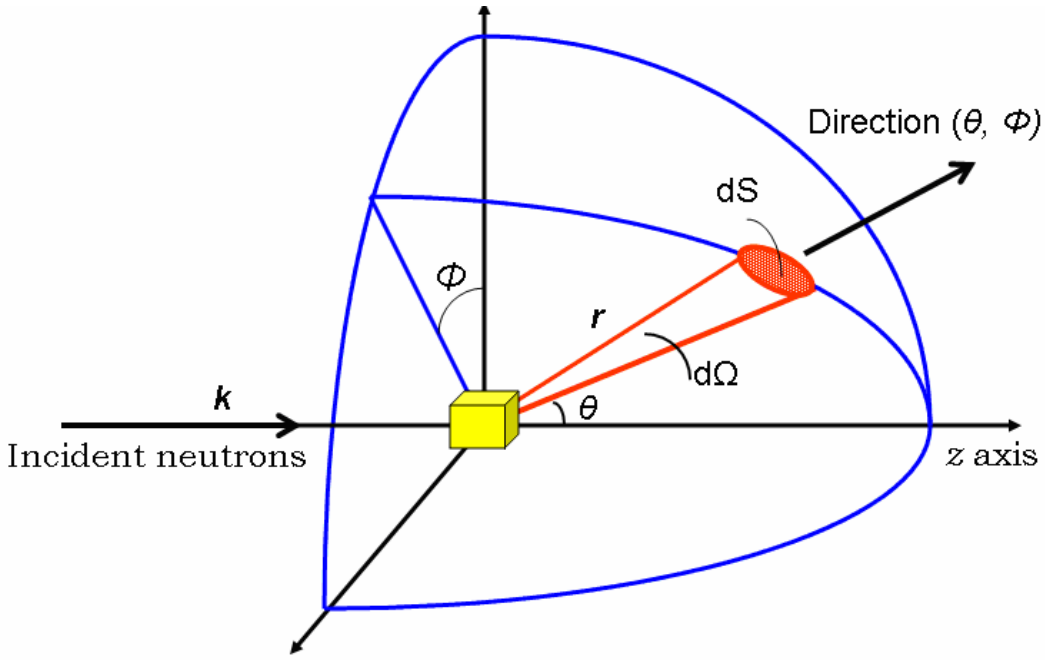

Figure 3.2: Geometry of a scattering experiment. In polar coordinates, (θ, ϕ) is the direction of the scattered neutrons; dΩ is the solid angle subtended by the counter at the target; the distance of the counter from the target is assumed to be large so that dΩ is well defined; Φ is the flux of incident neutrons.

Table 3.1: Scattering lengths and cross sections for different elements.

Element	Coherent Scattering Length b_c (fm)	Coherent Scattering Cross Section σ_c (barns)	Total Scattering Cross Section σ_T (barns)	Incoherent Scattering Cross Section $\sigma_i=\sigma_T-\sigma_c$ (barns)	Absorption Cross Section (λ=1.84 Å) σ_{abs} (barns)
H	-3.74	1.76	82.0	80.3	0.333
D	6.67	5.59	7.64	2.05	0.0005
C	6.65	5.55	5.55	0	0.003
N	9.36	11.03	11.53	0.5	1.91
O	5.80	4.23	4.23	0	0.0001
Ti	-3.44	1.49	4.36	2.87	6.09
B	5.30	3.54	5.24	1.70	767
Cd	4.87	3.04	6.50	3.46	2520
V	-0.40	0.02	5.11	5.09	4.9

3.3 Elastic scattering of neutrons

Both the coherent and the incoherent part of the total cross section are composed of an elastic and an inelastic term. Here only the results useful for understanding the technique used in this work are presented, avoiding any detailed derivation.

The final expression of the elastic coherent and incoherent differential cross section in the case of multi-atomic crystals can be written as:[19]

$$\frac{d\sigma}{d\Omega}_{coh}^{elast} = \left| \sum_{\ell} b_{\ell} e^{i\vec{Q}\bullet\vec{\ell}} \right|$$

$$\frac{d\sigma}{d\Omega}_{incoh}^{elast} = N \frac{\sigma_{incoh}}{4\pi}$$

In the first expression, $\vec{\ell}$ is the equilibrium position of each scatterer. As it can be seen, the incoherent part has no momentum dependence and therefore contributes to a diffuse background. On the other hand, the coherent part has momentum dependence and contributes to give information on the location of the scatterers. The term $\sum_{\ell} e^{i\vec{Q}\bullet\vec{\ell}}$ is the so called structure factor; it determines the positions of the Bragg peaks (elastic peaks).

3.4 Debye-Waller factor

The assumption that we made so far is that the atoms that constitute a crystal have a perfectly periodic and static arrangement. Real crystals, on the other hand, have various kinds of disorder. The atoms in the crystal vibrate at any given temperature. Thermal fluctuations of the atoms from their average position (displacements) are taken into account through the Debye-Waller factor. Considering this thermal disorder due to harmonic lattice vibrations, the resulting distribution of atomic displacements from the average position is a Gaussian. The Debye-Waller factor is an exponential factor that increases linearly with temperature for high temperatures; it can be written as $e^{-Q^2\langle\langle u^2\rangle\rangle}$,

where $\langle\langle u^2 \rangle\rangle$ is the r.m.s. amplitude of the lattice vibrations. The introduction of this correction factor translates into a decrement of the intensity of the Bragg peaks at high Q. The total scattering intensity of the crystal, however, is not diminished; the lost intensity goes to increase the thermal diffuse scattering, represented by the broad peaks in between two sharp Bragg peaks. While thermal fluctuations do affect the intensity of the elastic peaks, they do not contribute to their broadening. Since the incoherent elastic cross section is Q-independent, the Debye-Waller factor concerns only coherent elastic scattering.

3.5 Sources of neutron beams

Neutron scattering requires intense sources of neutrons. There are two possible sources of neutron beams suitable for a scattering experiment: nuclear reactors and accelerator-based sources (spallation sources).

In the first case, neutrons are produced by fission of heavy nuclei such as U_{235}. They are called fast neutrons and they usually have energies on the order of 1-2 MeV. Fast neutrons are slowed down by a process called moderation: they are forced to pass through a material, a moderator, until they reach a thermal equilibrium with the molecular motions of the material by repeated elastic collisions with the atomic nuclei. Commonly used moderators are H_2O, D_2O, LH_2, LD_2 because of their low A (atomic number) and their small σ_{abs}.

The moderation process gives neutrons with energies from the meV range to tenths of an eV. They are called slow (thermal) neutrons because their energies are significantly lower than the fast ones. Neutrons with energies well below the energy that they would have in equilibrium at room temperature (0.025 eV) are called cold neutrons (*table 3.2*). Given the energy range of thermal neutrons, their wavelengths are of the same order as inter-atomic distances (few Å); diffraction measurements are therefore possible.

Table 3.2: Classification of neutrons by their energies.

Neutrons	$E_{kinetic}$	T (K)	Velocity	Wavelength
UCN	~250 neV	~0.003	~7 m/s	~600 Å
Cold	<3 meV	<35	~760 m/s	~5 Å
Thermal	~25.9 meV	300	~2,224 m/s	~1.8 Å
Resonance	~1 eV	$\sim 10^4$	$\sim 1.4 \cdot 10^4$ m/s	~0.3 Å
Slow	~100 eV	$\sim 10^6$	$\sim 1.4 \cdot 10^5$ m/s	~0.03 Å
Intermed. Energy	~10 keV	$\sim 10^8$	$\sim 1.4 \cdot 10^6$ m/s	~0.003 Å
Fast	~1 MeV	$\sim 10^{10}$	~0.046 *c*	~0.0003 Å
High Energy	~100 MeV	$\sim 10^{12}$	~0.43 *c*	~3 fm
Relativistic	>1 GeV	$>10^{13}$	>0.875 *c*	<0.9 fm

In general, reactors produce a continuous flux of neutrons. The High Flux Isotope Reactor (HFIR) at Oak Ridge produces a continuous flux of ~ 1×10^{15} neutrons/cm^{2}s.

In the second case, neutrons are produced by bombarding a heavy target (U, W, Ta, Pb, Hg) with high-energy protons. The term spallation comes from the fact that, when fast high-energy protons bombard a heavy atomic nucleus, some neutrons are ejected, that is "spalled". For every proton striking a heavy nucleus of the target, 20 to 30 neutrons are expelled. An example is the SNS in Oak Ridge, where an ion source produces negatively charged hydrogen ions (a proton and two electrons). These ions, accelerated by a linear accelerator, are passed through a foil; in this way, two electrons are stripped off each ion, which is then converted into a proton. The protons pass into a ring that accumulates them in bunches. Each bunch of protons is then released as a high-energy pulse of protons. These pulses hit a target made of liquid mercury. In this way, through the spallation process, high-energy pulses of neutrons are obtained. These fast neutron pulses are slowed down in a moderator as described before and finally guided through the beam lines. Neutron pulses can be produced with a much higher intensity than that available from continuous sources. Each pulse produced by the SNS will

contain a neutron intensity 50 to 100 times higher than that obtainable from a continuous source. The availability of short and intense neutron pulses is particularly advantageous for the time of flight (TOF) analysis.

3.6 Measurement techniques

Two main measurement techniques are available at neutron scattering facilities: the triple-axis spectrometer (TAS) and the time of flight (TOF).

In the first case, a measurement is made for a single scattering vector and energy transfer: only the measure of a particular excitation at particular values of Q and E is possible at a time. A complete scan of a series of values is very time-consuming. The TAS is available at a reactor's neutron sources, where the flux of neutrons is continuous.

The TOF technique is most commonly performed at spallation neutron sources, which can produce neutron pulses with a significantly higher intensity than the one available from continuous sources. As a consequence, one of the main advantages of the TOF over the TAS resides in the possibility of accessing higher momentum transfer $\boldsymbol{Q}$. In real space analysis, this means having information on a shorter atomic-distance scale.

3.6.1 Triple-axis spectrometer (TAS)

A triple-axis spectrometer consists of three independently controlled axes of rotation: one for the monochromator crystal, one for the sample, and one for the analyzer crystal (*figure 3.3*). The three axes define three main steps:[22]

(1) Neutrons of a specific wavelength are extracted from the neutron beam - generated by a nuclear reactor - through a *monochromator crystal*, which may be turned about the first axis. Therefore the neutron beam diffracted from the monochromator and incident on the sample is monochromatic with a fixed initial energy and wavevector (E_i, K_i).

(2) Neutrons are scattered inelastically from the sample, which can rotate about a second

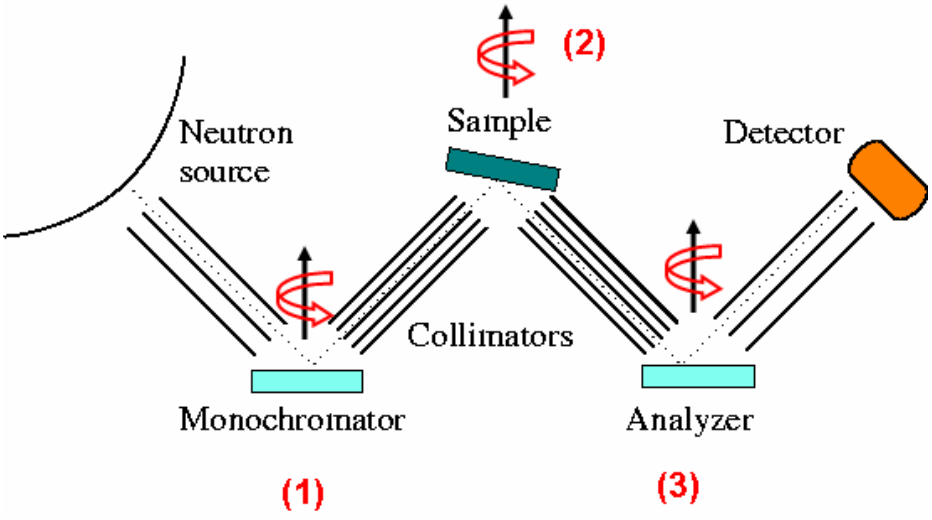

Figure 3.3: Schematic representation of a triple axis spectrometer for inelastic neutron scattering experiments. The source is a nuclear reactor.

axis. These scattered neutrons possess a distribution of final energies E_f and final wave vectors K_f.

(3) The analyzer (third axis) is aligned in order to reflect neutrons of a specific energy and a specific wavevector onto the detector; the analyzer can provide a wavelength selection with an accuracy of $\Delta\lambda/\lambda \sim 10^{-3}$.

The triple-axis spectrometer is able to measure the intensity of scattered neutrons for a particular momentum transfer $\boldsymbol{Q}$ and energy transfer $E=\hbar\omega$. Usually the measurements are done keeping either K_i or K_f fixed. With a computer-controlled spectrometer, there are two possible scan modes: constant-Q and constant-E scans. In the first case, it is possible to scan the energy transfer for a selected specific point in reciprocal space. In the second case, when the energy transfer is maintained constant, it is possible to scan along a particular direction in reciprocal space. One limitation of the TAS is that a measurement can be performed only in a restricted range of values of $\boldsymbol{Q}$ and E. Furthermore, a large portion of scattered neutrons is lost undetected.

When the neutrons penetrate the sample, they can initiate or cancel out oscillations in the atoms of the sample (phonons). If neutrons manage to create (excite) phonons, they themselves lose energy (inelastic scattering). Thus, using the TAS, it is possible to chart the atomic dynamics of a material, diffusion movements in liquids, and fluctuations in magnetic material.

3.6.2 Time of flight (TOF) measurement

The time of flight (TOF) is the technique used in this research. There are three basic steps:[21]

(1) A pulse of polychromatic neutrons is produced. Neutrons with different wavelengths and energies are available; those with higher energy have shorter wavelengths.

(2) Neutrons spread out in time. Letting the neutrons travel along a short distance from the moderator to the sample, it is possible to separate them according to their energies. Neutrons with higher energy reach the sample sooner than neutrons with lower energy; a wide spectrum of energies irradiates the sample (*figure3.4a*).

(3) After interacting with the sample, neutrons will gain or lose energy. The result is a change in their velocity. A multi-detector records the scattering angles and the times of arrival of the scattered neutrons (*figure 3.4b*). The result is the pattern of peaks shown in *figure3.4c*. Since thermal neutrons of all energies are available for use, the time-of-flight technique enables the collection of many data points for each source pulse reaching the sample.

Even if a spallation source is particularly suitable for the TOF, also a reactor source can be successfully used. In this case, after a monochromator selects a wavelength, a pulsed beam is generated using a combination of choppers.

A schematic representation of a TOF spectrometer is shown[23] in *figure 3.5*.

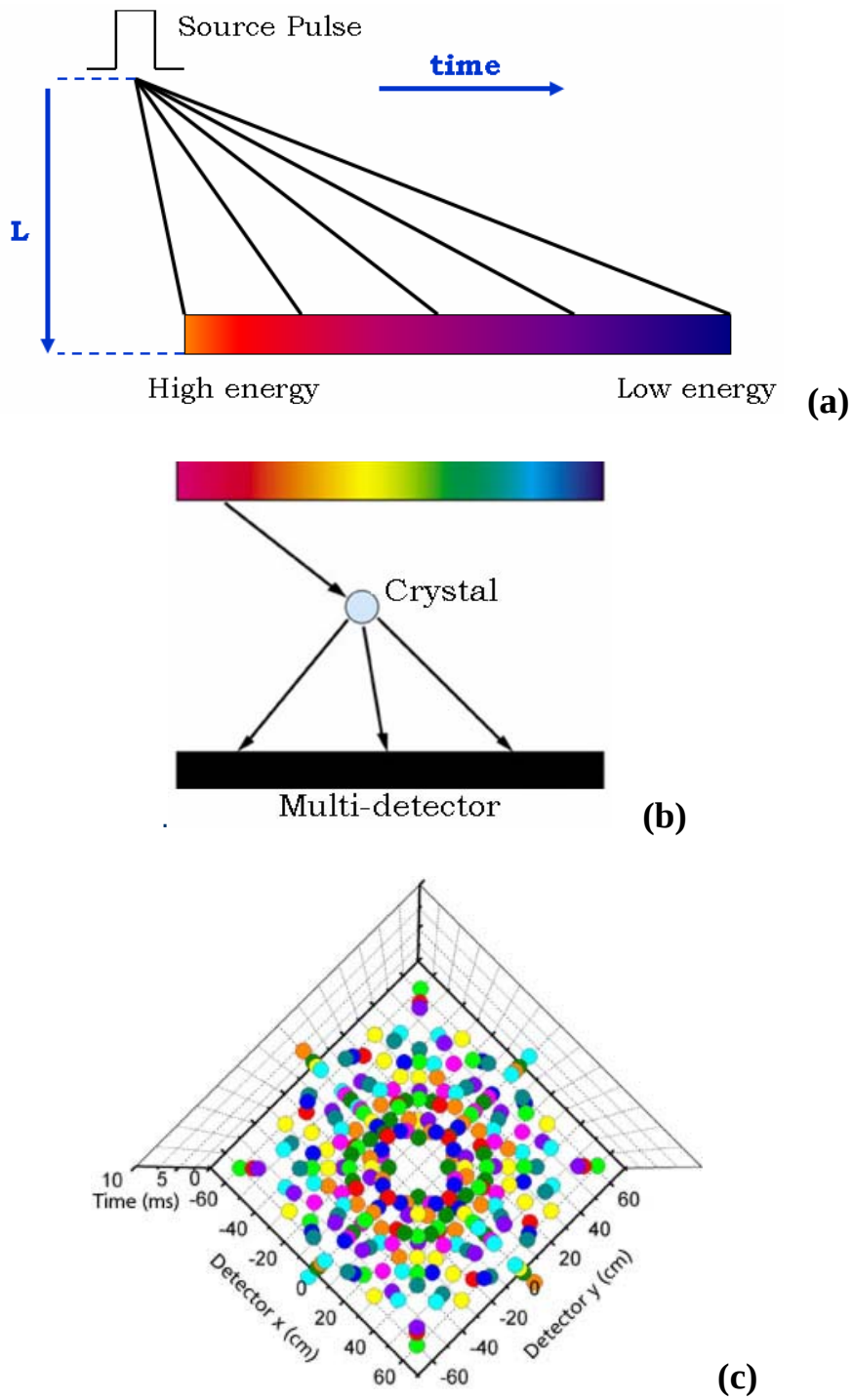

Figure 3.4: Schematics of a Time of Flight Technique (TOF) measurement. (a) Neutrons travel along a path L of several meters and are separated in energy. (b) A multi-detector records the times of arrival and the positions of the neutrons scattered from the sample. (c) Pattern obtained from the multi-detector for a crystal of the superconductor $YBa_2Cu_3O_{7-\delta}$.

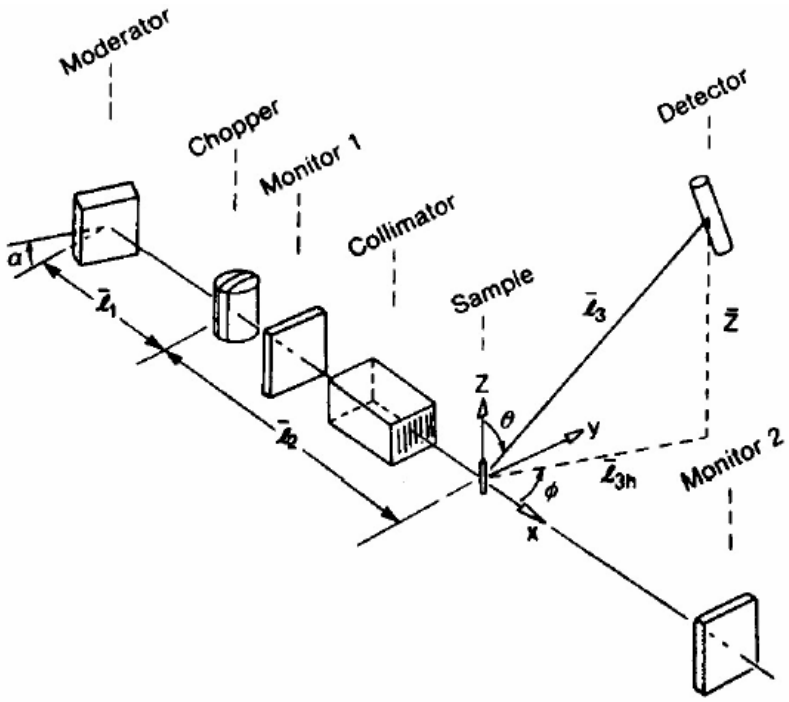

Figure 3.5: Schematic diagram of a TOF spectrometer. The rotating chopper has the task of selecting neutrons with the desired velocity, i.e. with the desired wavelength.

The main factors that affect the resolution function in the case of the TOF are related to both the instrument and the sample. The three main factors are: the source pulse width; the ambiguity in the measure of the flight distances to and from the sample due to the sample size and to the detector size; and the chopper opening time. Another important issue about the instrument resolution that must be considered is the uncertainty in the energy that results in an uncertainty in the momentum transfer.

3.7 Time of flight neutron powder diffraction

Powder diffraction is one of the most widely used techniques to explore the structural properties of materials. Powder samples are polycrystalline and, ideally, the micro crystallites are randomly oriented. Contrary to a single crystal experiment, individual diffraction spots are not observed; instead, what we observe is a series of rings of diffracted intensity as a function of the momentum transfer. The geometry of a powder

diffraction experiment is schematically represented in *figure 3.6*. When a monochromatic beam of neutrons with wave vector ***k*** is incident on a powder sample, the scattered wave vector ***k'*** lies in a cone, called the Debye-Scherrer cone. Only crystallites whose ***τ*** vectors lie on a cone with axis along k and semi angle ψ contribute to the scattering. The expressions valid for ψ and ***τ*** can be written as:

$$\Psi = \frac{1}{2}\pi - \frac{1}{2}\theta \quad \text{and} \quad |\vec{\tau}| < 2k$$

While earlier diffraction experiments have been done using continuous sources, in the last years, time-of-flight powder diffraction experiments using a spallation source have become practicable. Since this technique utilizes a white beam (non monochromatized beam) of neutrons, it is possible to use the whole neutron flux, without having the neutron loss that normally happens during the process of monochromatization. Furthermore, the use of spallation sources gives the possibility to access high values of the momentum transfer through high-energy neutrons. This property of a spallation source is particularly important in real-space refinement analysis, where high-**Q** information translates into low-range distance information.

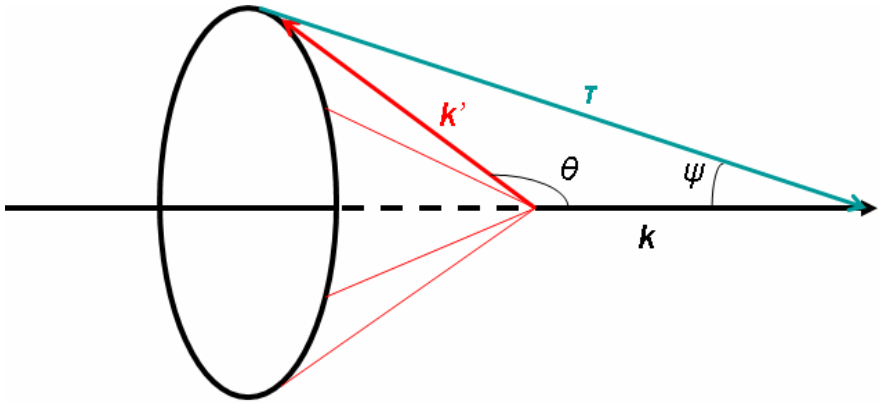

Figure 3.6: Geometry of a powder diffraction experiment: the Debye-Sherrer cone. The incident wave vector is ***k***, while the scattered wave vector is ***k'***.

Momentum information can be gathered from the total time of flight of a neutron and the scattering angle θ using the following relation:

$$Q = \frac{2\pi}{d} = \frac{L_1 + L_2}{\Delta t}\frac{2m_n \sin\theta}{\hbar}$$

L1 and L2 are, respectively, the primary flight path (moderator-sample) and secondary flight path (sample-detector); Δt is the total time of flight; m_n is the neutron mass.

Even though only elastic scattering is supposed to be observed, a real diffraction spectrum includes some inelastic contribution to the total intensity due to the fact that no energy analyzer is used. As a result, inelastically scattered intensity may be interpreted as elastic intensity with the wrong momentum transfer. In the case of Rietveld analysis, this does not represent a major problem since the inelastic part of the total intensity contributes only to the broad featureless background. In the case of real space refinement, however, also the background is taken into account when we Fourier transform the whole diffraction spectrum. Appropriate corrections are needed. A well-known solution for this problem has been proposed by Plazcek.[19]

3.7.1 NPDF at LANSCE

In this thesis, measurements have been taken at the Neutron Powder Diffractometer (NPDF) at the Los Alamos Neutron Science Center (LANSCE). The NPDF is specifically designed for Pair Distribution Function (PDF) studies of disorderly and nanocrystalline materials.[26] In just a few hours, it is possible to collect a data set suitable for PDF analysis. The primary flight path is 32 meters and the secondary flight path is 1.5 meters. There are 20 detector panels with a total of 160 position-sensitive detectors in the backscattering region of the instrument. The medium and high angle backscattering detector banks determine a wide solid angle coverage; the extent of the range of the accessible momentum is enhanced by the backscattering geometry. *Table 3.3* shows the specifications of the NPDF diffractometer, while *figure 3.7* shows a schematic representation of the detector banks.

Table 3.3: Specifications of the NPDF diffractometer at LANL.

Specifications			
Moderator	chilled water (283K)		
Flight path	primary=32 m; secondary=1.5 m		
Beam size	5 cm high x 1 cm wide		
Detector Bank Info			
Bank	90	119	148
d-spacing	0.17-4.2 Å	0.14-3.4 Å	0.12-3.0 Å
Q	1.5-37.6 $Å^{-1}$	1.8-45.8 $Å^{-1}$	2.1-51.1 $Å^{-1}$
Measured **d**/d	0.31%	0.28%	0.15%
Detector type	124 ^{3}He tubes	80 ^{3}He PSDs	80 ^{3}He PSDs
Pixels	124	4000	4000
Pixel size (w x h)	0.5“ x 12“	0.5“ x 1.0“	0.5“ x 1.0“

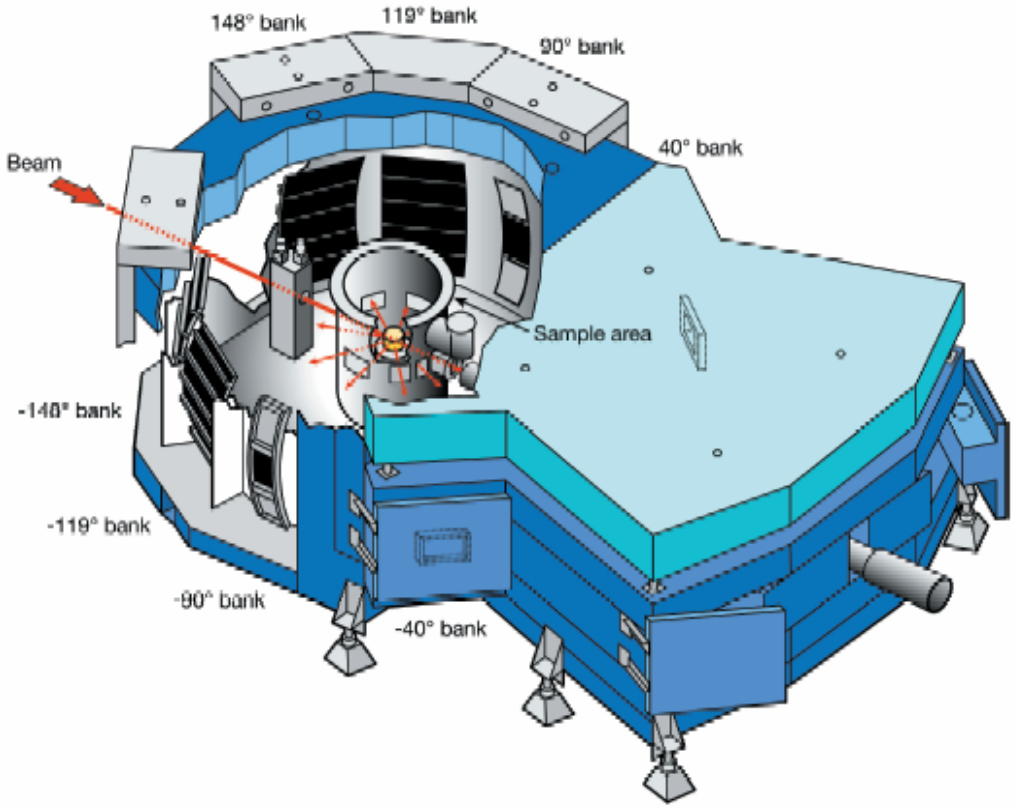

Figure 3.7: Schematic representation of the detector banks of the NPDF diffractometer.

At the ±148º detector banks, the maximum momentum transfer available is beyond 50 $Å^{-1}$. In practice, such a high limit yields great statistics for the momentum transfer range beyond 30 $Å^{-1}$; this feature turns out to be extremely advantageous for a high-resolution real-space refinement analysis.

3.8 Pair Distribution Function (PDF) technique

The Pair Distribution Function (PDF) technique is a method of analyzing diffraction data that provides a structural characterization of both crystalline and non crystalline materials. For a long time, it has been applied to materials without any structural periodicity such as liquids and glasses; only recently has it been used to study the atomic-scale structure of crystalline materials with large intrinsic disorder.[24]

The PDF technique uses the complete diffraction pattern and it is said to be a *total scattering* method. Standard crystallography collects long-range structural information from the position and the intensity of the Bragg peaks that constitute the diffraction pattern; on the other hand, the PDF technique collects structural information taking into account both the contribution of the Bragg peaks *and* the diffuse scattering - i.e. the broad peaks between two sharp Bragg peaks. The fact that PDF takes into consideration the diffuse scattering represents a significant advantage with respect to conventional crystallography, since local deviations from the average structure are indeed related to the diffuse scattering.

3.8.1 Standard crystallography vs. PDF

In traditional crystallography, a crystal is defined as a three dimensional periodic arrangement of atoms with translational periodicity along the three dimensions of space (called principal axes). It is possible to generate an infinite crystalline structure by filling the space with the so-called unit-cells. The process of determining the atomic structure of

a crystal consists, therefore, of locating the average position of the atoms within one unit cell. Information about atomic positions is given by the study of the Bragg peaks.

As already discussed, atomic thermal fluctuations from the average position (displacements) are taken into account through the Debye-Waller factor, which has the effect of decreasing the intensity of the Bragg peaks. The intensity lost from the Bragg peaks goes to increase the diffuse scattering. As a consequence, the information gathered from the Bragg analysis is only about the average position of individual atoms. The distance between the average positions is considered a good estimate of the average inter-atomic distance.

Crystallography has been, and still is, an incredibly successful method for the structural characterization of materials. However, real materials do not have the long-range order and the perfect periodicity of a crystal; they are, instead, disordered or partially disordered. Since deviations are mainly responsible for their physical properties, the more a material deviates from being perfectly periodic, the more the role of the diffuse scattering becomes crucial. In the PDF analysis, no assumption of periodicity of any kind is made; a wide range of materials, from completely disordered to crystalline, can be studied.

3.8.2 Atomic pair distribution function

The Pair Distribution Function (PDF) technique is based on the Fourier analysis of the total scattering – the scattering that includes Bragg scattering, elastic diffuse scattering, and inelastic scattering. The physical quantity of interest is the measured intensity of the total scattering S(Q), called the total scattering structure function. Since a diffraction pattern appears as intensity versus momentum transfer Q=($K_f - K_i$) in the reciprocal space, the quantity S(Q) is easily accessible. There are two main steps in a PDF analysis:[25]

(1) Raw data from a diffraction measurement are corrected for various instrument and sample effects (sample absorption, multiple scattering, polarization, extraneous

background signals…); data must also be normalized to give a set of final data on an absolute scale.

(2) Corrected and normalized data are Fourier transformed to real space. The sine Fourier transform of the reduced structural function Q[S(Q)-1] gives the so-called *reduced pair distribution function*, *G(r)*, which depends only on the distance *r* between two atoms in real space:

$$G(r) = 4\pi r(\rho(r) - \rho_0) = \frac{2}{\pi}\int_0^\infty Q[S(Q) - 1]\sin(Qr)dQ$$

In the above expression, ρ_0 is the average number density of atoms, $\rho(r)$ is the distribution of the inter-atomic distances (called the *atomic pair density function*), and S(Q) is the previously introduced total scattering structural function. The main steps of the PDF analysis are shown in *figure 3.8*.

Because of experimental limitations on Q, G(r) is not the exact sine Fourier transform of the reduced structural function *Q[S(Q)-1]*. Data can be collected only within a finite range of the momentum transfer [0, Q_{max}]. The higher Q_{max}, the higher the real space resolution. Having high momentum scattering data is crucial for an accurate PDF analysis. Synchrotron X-ray and spallation neutron sources are capable of providing Q high enough to reveal local structural features with great accuracy. In practice, the problem that diffraction measurements can be taken only up to a certain Q_{max} results in termination ripples in the Fourier transform. One possible way to solve the problem of termination ripples is to consider a multiplying modification factor W(Q) that goes smoothly to zero for $Q>Q_{max}$. This costs, however, a broadening of the peaks.

The fact that we use a Fourier transform implies that the PDF permits the study of local structures in real space instead of in reciprocal space. In other words, the PDF analysis is simply another way to represent the diffraction data in real space. The advantage is that we can get real inter-atomic distances from the PDF peaks in a straightforward way; they give direct distances between pairs of atoms. If a peak shifts to a lower value of r(Å), for example, it follows that the bond between the two atoms has became shorter.

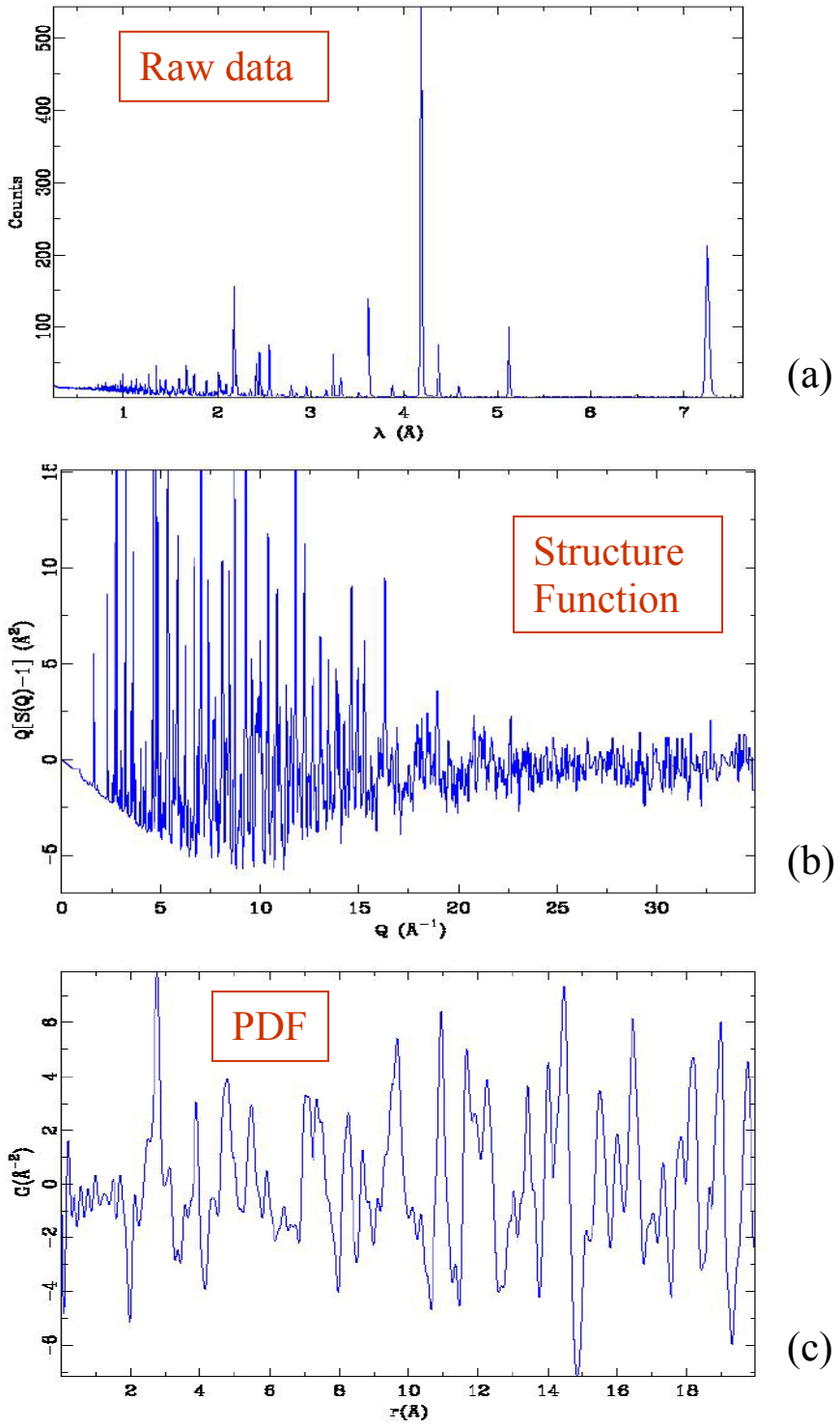

Figure 3.8: Main steps that lead to the final PDF spectrum. In this case the sample is Ni. **(a)** Raw data are the result of a diffraction experiment; **(b)** we consider corrections to the raw data due to experimental effects and we put them on an absolute scale; **(c)** finally we take the Fourier transform of the properly corrected and normalized data.

The PDF analysis can be applied to diffraction data obtained using neutrons, electrons, and x-rays. Powder and single crystal methods are both valid. However, powder measurements are significantly easier to perform. Since arbitrary fitting parameters are not involved, theoretical calculations and experimental data can be directly compared.[27, 28]

In theory, obtaining a three dimensional PDF is also possible. All we need is to collect diffraction data in three dimensions. The measurement is, however, very time consuming. For this reason, PDF is usually applied to isotropic samples (powder diffraction); in this way *G(r)* is reduced to a one dimensional function.[24]

The PDF function is also referred to as a *pair correlation function.* The term *correlation* is used to mean deviation from the average structure. In this context, correlations mean the oscillations of the PDF. The atomic structural information is contained in these oscillations.

3.8.3 Various correlation functions

We have already introduced one correlation function, the *reduced pair density function G(r)*; this function is directly obtained from the Fourier transform of $S(\boldsymbol{Q})$ and thus is directly related to the data. In this paragraph, we will introduce other correlation functions, each with its own physical peculiarities.

The original definition of *pair density function* (PDF), ρ(r), is given by:

$$\rho(r) = \frac{G(r)}{4\pi r} + \rho_0$$

where ρ_0 is the average atomic number density.

In addition to *G(r)* and ρ(r), we can also define a *radial distribution function* (RDF), *R(r)*:

$$R(r) = 4\pi r^2 \rho_0 g(r)$$

In the expression of *R(r)*, the function *g(r)* is defined through ρ(r) in the following way:

$$\rho(r) = \rho_0 g(r)$$

g(r) is called *pair distribution function* and is related to the *reduced distribution function G(r)* by:

$$G(r) = 4\pi\, r\rho_0\big(g(r)-1\big)$$

Since $g(r) \to 1$ when $r \to \infty$ and $g(r) \to 0$ when $r \to 0$, then $G(r) \to 0$ when $r \to \infty$ and $G(r) \to -4\pi\, r\, \rho_0$ when $r \to 0$. This result is important because it implies that at low *r*, the function G(r) is a straight line going through the origin with a slope proportional to average number density ρ_0. A significant consequence of this fact is that while it is necessary to assume a certain value for ρ_0 when calculating *g(r)* or *ρ(r)*, in the case of *G(r)*, the information about ρ_0 is already contained in G(r) itself. Nothing concerning the structure is assumed in G(r).

An important feature of G(r) is that the random uncertainties in the data are constant in *r* and do not fall off like $1/r$ as in the case of *ρ*(r). G(r) is, therefore, extremely convenient for the purpose of refinement analysis of short range correlations since it does not suffer from the problem of giving statistically unjustified importance to the data at low *r*.

Considering the RDF, we can easily get the number of atoms in a spherical shell of thickness *dr* at distance *r* from a reference atom. The *coordination number*, in fact, is given by:[24]

$$N_{coord} = \int_{r2}^{r1} R(r)dr$$

where r_1 and r_2 identify the coordination shell of interest and, at the same time, the PDF peak. In other terms, the coordination number is obtained by integrating the intensity under a certain PDF peak. The RDF can be defined as the probability of finding an atom in an area of radius *r*.

What is notable is that the radial distribution function represents the actual distribution of distances seen from a particular atom. Therefore, here is where the Gaussian broadening due to thermal fluctuations or random disorder should be directly applied. The disadvantage of RDF is that it diverges like r^2: plotting the data using *R(r)* becomes less and less satisfactory as *r* increases.

In this work, refinement analysis was not explicitly performed; therefore, we opted to use $\rho(r)$ and *RDF*(r), instead of G(r). The convenience of this approach resides in the fact that, since $\rho(r)$ has a natural baseline at $\rho(r) = 0$, the use of *RDF* permits a direct comparison between the respective weights of neighboring peaks.

3.8.4 Experimental considerations on neutron PDF measurements

Ideally, in order to carry out the Fourier transform of S(Q), measurements up to $Q = \infty$ would be necessary. In practice, the termination value $Q=Q_{max}$ implies that what we carry out is a Fourier transform that utilizes a cut-off function of S(Q). The consequence is the appearance of the so called termination ripples, spurious oscillations of the data at short distances. However, for high Q_{max} the termination errors can be considered negligible. In fact, since $S(Q)\rightarrow 1$ for increasing Q, if S(Q)-1 is small enough at Q_{max}, the effect of the termination in the Fourier transform is minimal.[24] The choice of Q_{max} is, therefore, of a great importance in a PDF measurement. Furthermore, because the PDF is obtained via Fourier transform of the scattering data, the extent of the data in *Q*-space determines the real space resolution of the PDF. In other terms, the required real space resolution of the PDF determines the value of Q_{max} that is necessary in a measurement.

The effect of the Q resolution ΔQ is also a key factor in a PDF measurement. *Figure 3.9* shows an example of this effect. Two different instruments were used to measure nickel powder, the GLAD at IPNS and the NPDF at LANSCE.[26] The first diffractometer has a low resolution of ~0.6%, the second has a higher resolution of ~0.15%. In both cases, data were terminated at Q_{max}=35 $Å^{-1}$. It is clear that information is lost in the nanometer range when a low resolution diffractometer is used. Moreover, the *Q* resolution results in an exponential dampening of the PDF peaks as function of *r*.[30] In order to determine a pair distribution function over a large distance-range, a high Q resolution is essential. In a measurement, the desired maximum range of distances determines the necessary ΔQ. NPDF permits high *Q*-resolution data acquisition for PDF analysis up to *r*~100 Å.

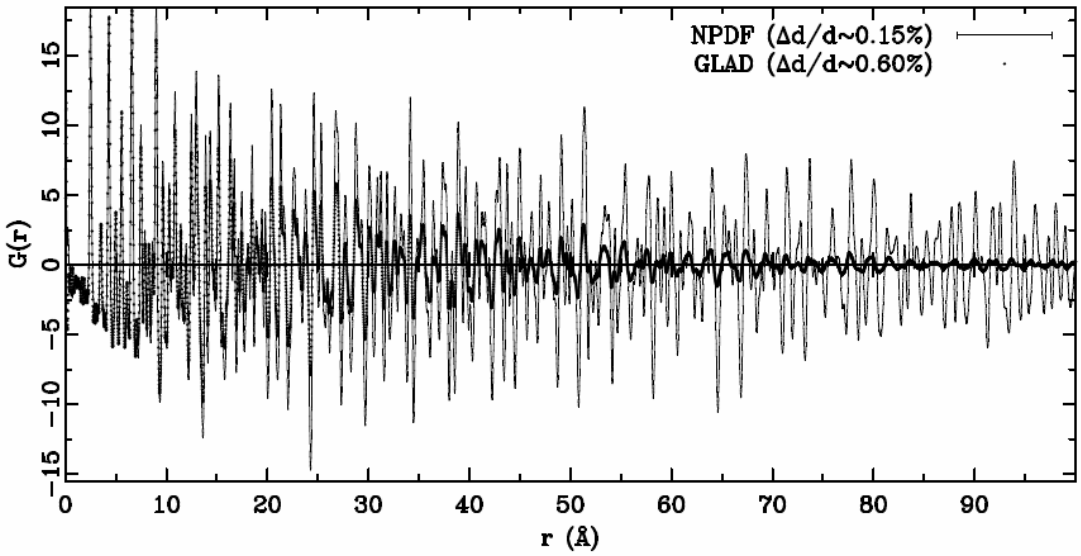

Figure 3.9: Influence of the reciprocal space resolution ΔQ on the PDF of Ni. The solid line represents data from NPDF at Lujan Center at Los Alamos National Laboratory and the dots are data from GLAD at Intense Pulsed Neutron Source at Argonne National Laboratory.

Chapter 4

Properties of the compounds studied

In this chapter, the main properties of the compounds studied and the sample preparation are discussed. Since the three main characters in the unfolding novel of superconductivity in sodium cobaltate are (1) the non superconducting anhydrous compound Na_xCoO_2, (2) the deuterated superconducting compound $Na_xCoO_2yD_2O$, and (3) (heavy) water, a brief 'biographical' sketch of each of them is presented here before discussing the experimental results in the next chapter.

4.1 Structure of Na_xCoO_2

Sodium cobalt oxide Na_xCoO_2 has a triangular layered structure identified by several space groups, depending on the Na content (x).[29] Here only the composition with x~0.7 is discussed.

The crystal structure of the non superconducting $Na_{0.7}CoO_2$ is a layered structure characterized by the hexagonal space group *P63/mmc*.[1] Two dimensional CoO_2 layers, perpendicular to the c axis, alternate with layers of Na^+ ions. Co atoms form a triangular lattice due to the fact that each CoO_2 layer is arranged in a pattern of edge-sharing octahedra. CoO_2 layers have a 6_3 screw-axis symmetry and along the c axis there is mirror symmetry between two CoO_2 layers. Na^+ ions are in two partially occupied sites, Na1 and Na2 (*figure 4.1a*). The Na1 site is coordinated to six oxygen atoms, three above and three below its site; each O atom is coordinated to a different Co atom. Also the Na2 site is coordinated with six oxygen atoms, but in this case, these O atoms are coordinated only to two Co atoms, one above and one below its site[5] (*figure 4.1b*).

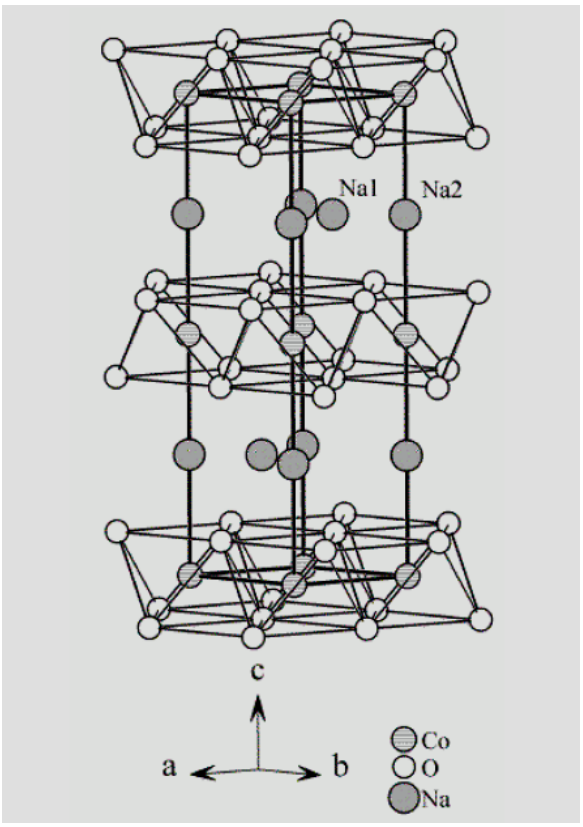

(a)

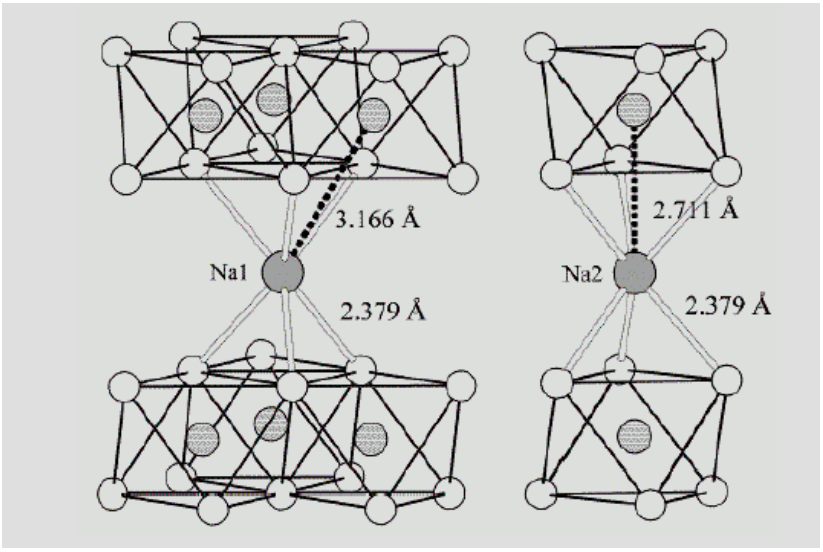

(b)

Figure 4.1: (a) Structure of $Na_{0.7}CoO_2$ (space group P63/mmc). Layers of edge-sharing CoO_6 octahedra are separated by layers of Na^+ ions. Na atoms are in two partially occupied sites (Na1 and Na2). **(b)** Coordination of the Na1 and Na2 sites to O atoms in the CoO_2 layer.

Different research groups have determined the lattice parameters of $Na_{0.7}CoO_2$ using Rietveld refinement on both neutron[4,5] and x-ray[2] diffraction data at different temperatures. In the case of powder neutron diffraction data, the results of this analysis are summarized in *table 4.1*. The calculated PDF of $Na_{0.7}CoO_2$ used in this thesis is based on the structure obtained by this particular Rietveld refinement.[5]

4.1.1 Phase diagram of Na_xCoO_2

As already mentioned in chapter two, Na_xCoO_2 possesses an interesting phase diagram[31,3,32,33], not yet completely understood. The superconducting phase - the one directly related to this work - appears for a narrow range of doping ($1/4<x<1/3$), when water is intercalated.[1] T_C is >2 K with a maximum of 4.5 K at x~0.3. The dome-like behavior in this doping interval resembles that of cuprates. As x increases, first a paramagnetic phase ($1/3<x<1/2$) and then a charged ordered insulating phase (x~1/2) appear. For x~2/3 the system behaves like a Curie-Weiss metal[3,34], while for x~3/4 a magnetically ordered metallic phase sets in; the latter phase is believed, but it is still not certain, to be equivalent to the spin-density-wave (SDW) phase. The described phase diagram is illustrated in *figure 4.2*.

For a general Na content x, the site occupancies of the Na atoms are inequivalent and vary systematically with x. The values x=1 and x=1/2 correspond to two special situations. In the first case, one site is fully occupied while the other one is empty; in the second case, both sites have equivalent occupancy (1/4) and the system behaves like a charged ordered insulator.

Table 4.1: Lattice parameters for Na_xCoO_2 (x~0.7) based on Rietveld refinement of powder neutron diffraction data at two different temperatures.[5]

Temperature	12 K	295 K
a (Å)= ***b*** (Å)	2.83176	2.83287
c (Å)	10.8431	10.8969

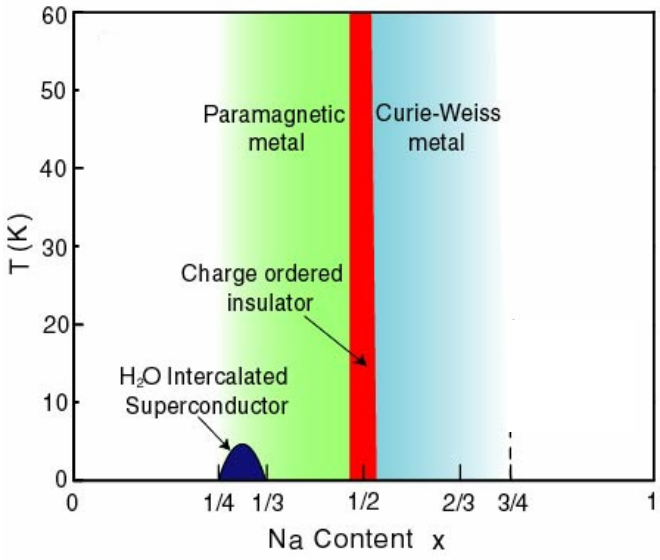

Figure 4.2: Phase diagram of Na_xCoO_2. The superconducting state appears for a narrow interval of the doping, $1/4<x<1/3$. When $x\sim1/2$, Na_xCoO_2 behaves like a charge order insulator, like a paramagnetic metal when x is just below 1/2, and like a Curie-Weiss metal when x is just above 1/2. For $x\sim3/4$, some believe that it behaves like a SDW metal.

4.2 Structure of $Na_xCoO_2yD_2O$

$Na_{0.7}CoO_2$ is made superconducting by partially removing Na ions and subsequently intercalating water.[1] When the sodium concentration is reduced, Na is selectively removed from one of the two partially occupied sites; the site that undergoes the strongest Na-Co repulsion is emptied, while the occupancy of the other site is decreased to ~1/3. During this process, the oxidation state of Co changes. Therefore, as in cuprates, the doped charge originates from the layer outside the CoO_2 plane (the Na layer). The intercalated water goes presumably to form additional layers between the Na and the CoO_2 layers, increasing the spatial separation between two successive CoO_2 planes (*figure 4.3*). This increment can be noticed by considering the difference in the value of the *c* axis; after water is inserted, *c* almost doubles.

Several neutron and X-ray diffraction experiments have been conducted in order to investigate the crystal structure of $Na_xCoO_2yD_2O$.[1,4,5,35] The values of the lattice parameters found by Rietveld refinement are reported in *table 4.2*.

Table 4.2: Lattice parameters for $Na_xCoO_2yD_2O$ based on Rietveld refinement of powder neutron diffraction data at two different temperatures.[5]

Temperature	12 K	295 K
a (Å)= ***b*** (Å)	2.81693	2.82166
c (Å)	19.6449	19.7681

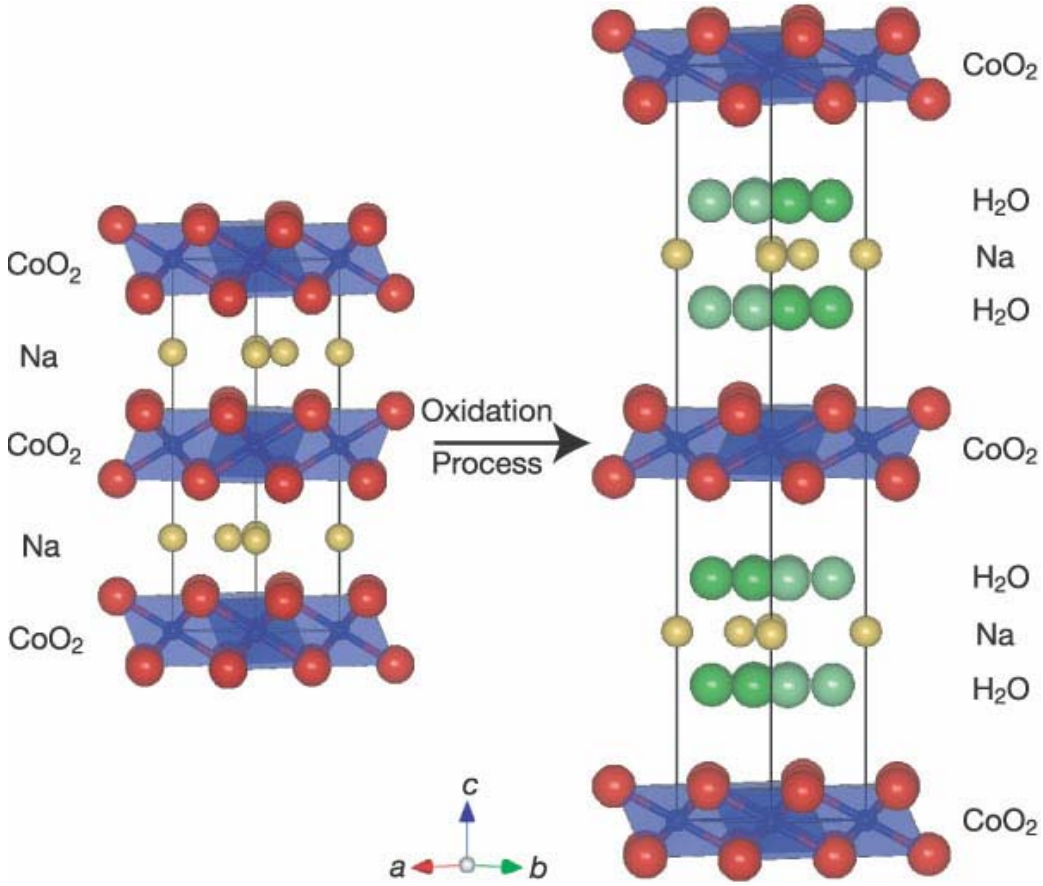

Figure 4.3: Oxidation process in sodium cobaltate. When water is intercalated in the Na deficient compound Na_xCoO_2, the spatial separation between CoO_2 layers is increased by the formation of additional H_2O layers between two consecutive Na and CoO_2 layers.

Despite many efforts, however, no agreement on the spatial distribution of the H_2O (or D_2O) molecules has been reached yet. By means of neutron scattering, it has been argued that the water layer resembles the low temperature ice structure.[4]

Up to this point, the most likely arrangement of the water molecules within the structure of $Na_xCoO_2yD_2O$ has been proposed by Jorgensen et al.[5] According to their model, the maximum T_C of 4.5 K is achieved by coordinating each remaining Na atom to four different D_2O molecules, two above and two below the Na site.

One D atom of each water molecule is hydrogen bonded to an O atom belonging to a CoO_2 plane; the second D atom of each water molecule is positioned in a plane between the Na and the CoO_2 layers and is hydrogen bonded to the O atom of a neighboring D_2O molecule (*figure 4.4*). The formation of these hydrogen bonds between adjacent D_2O molecules within the water planes leads to the formation of D-O---D-O---D-O chains characterized by a zigzag pattern. The D-D distance in these chains is 2.44 Å (*figure 4.5*).

One of the criteria used to select the 4-fold coordination of Na to D_2O molecules regards the average Na-O distance; this model, in fact, keeps its value (2.31 Å) close to the value assumed in the parent compound (2.41 Å). In addition, all the positions assumed for the D_2O molecules allow the formation of hydrogen bonds that involve both the D atoms of each molecule. Moreover, the orientation chosen for the D_2O molecules is the orientation that tends to minimize the Na-D and D-D repulsion. In particular the constraint on the Na-D distance gives rise to an arrangement of sodium and water in a two dimensional super-cell. The smallest super cell that preserves the hexagonal symmetry of the parent compound has been found to be an orthorhombic super cell with dimensions $(3a, \sqrt{3}\,a, 3c)$ (*figure 4.5*). This structure has 1/3 of the Na sites occupied; four O atoms are coordinated to each Na^+, two above and two below the ion. The resulting ideal composition is $Na_{1/3}CoO_2(4/3)D_2O$; for this composition, T_C assumes its maximum value of 4.5 K.

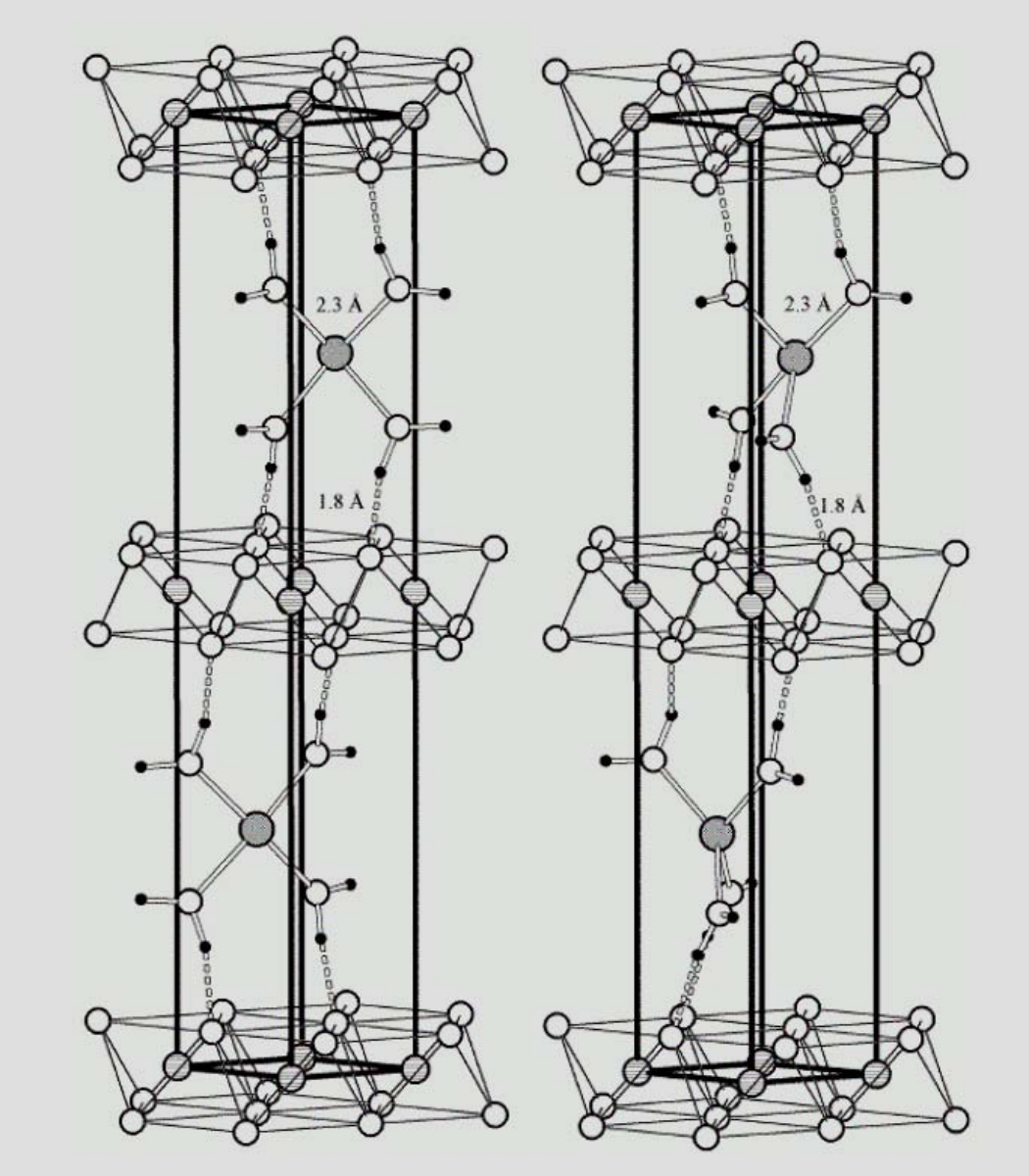

Figure 4.4: The structure model of $Na_xCoO_24xD_2O$ ($x\approx1/3$) proposed by Jorgensen et al. Two arrangements are possible, the *cis* (planar) and the *trans* (twisted by 60°). Each of them corresponds to a possible arrangement of the D_2O molecules above and below a certain Na^+. So far, diffraction experiments could not distinguish between the two.

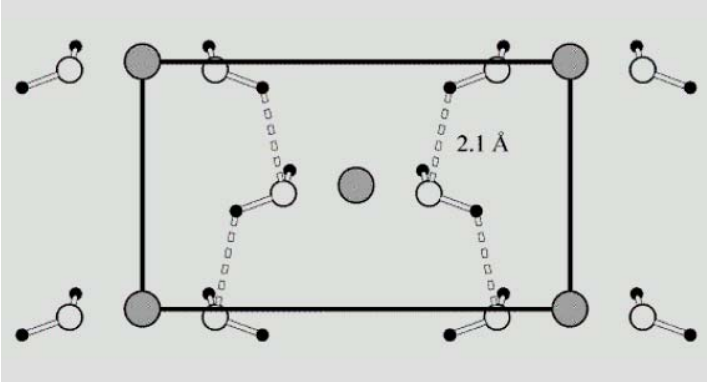

Figure 4.5: Two dimensional super-cell in $Na_xCoO_2 4xD_2O$. In the Jorgensen model, sodium and water molecules are arranged in a two dimensional super-cell of dimensions $3a \times \sqrt{3}\, a \times 3c$. The zigzag chains D-O---D-O---D-O due to the hydrogen bonds between adjacent D_2O molecules are here clearly visible.

4.3 Water and ice

The chemical formula of water is probably the most well known of all chemical formulas. One molecule of water consists of 2 atoms of hydrogen and one atom of oxygen linked together by covalent bonds. For a free molecule, commonly used molecular models utilize O-H lengths between 0.957 Å and 1.00 Å, and H-O-H angles from 104.5° to 109.5°; some of the values deduced by experiments and ab initio calculations are reported in *table 4.3*. This table shows that in liquid water, there are slightly greater values for both the H-O distance and the H-O-H angle; this happens because the hydrogen bonding between molecules slightly weakens the covalent bonding present within a molecule. In different H-bonded environments and in situations where the water molecules are bound to solutes and ions, the bond lengths and angles are likely to change due to a shift in the polarization of the molecules.[38]

Water molecules are rather symmetric. Two mirror planes of symmetry exist: one plane contains all three atoms, the other is perpendicular to the plane passing through the bisector of the H-O-H angle. Moreover, if a rotation of 180° about the bisector occurs, the shape of the molecule remains unchanged: the molecule has a 2-fold rotation axis (180°=360°/2).This type of symmetry belongs to the point group C_{2v}.

Table 4.3: Experimental values of the bond angle H-O-H and bond length O-H.

Technique	From the rotational components of the rotation-vibration spectrum (1956)	Neutron diffraction	*ab initio* calculations
O-H (Å) liquid	0.9572[42]	0.970[39]	0.991[41])
H-O-H (º) liquid	104.52[42]	106[39]	105.5[41])
O-H (Å) gaseous			0.95718[40]
H-O-H (º) gaseous			104.474[40]

Water molecules are arranged in a slightly distorted tetrahedral ordering. The value of the H-O-H angle is close, in fact, to the angle expected for sp_3 hybridization, the combination of one *s* orbital and *3p* orbitals. In an H_2O molecule, the four orbitals are oriented tetrahedrally: O is at the center of the tetrahedron, with two corners occupied by H atoms and two by the lone pairs, the electrons not involved in the covalent bonds. Such an ideal structure should give an H-O-H bond angle of 109.5°. However, the actual value for a free water molecule is 104.5º. This is due to the fact that the value of the H-O-H bond angle is determined by the force balance between the lone pair electrons on the oxygen and the hydrogen atoms. Since the lone pairs remain closer to the O atom, the repulsion between them ends up being stronger than the repulsion between the two covalent-bonding pairs. As a result, the H atoms are forced to get closer. Therefore, the final value of the H-O-H bond angle is less than the one that would emerge from a perfect tetrahedral structure, and it turns out to be 104.5º.

The fact that the molecule is bent is of a crucial importance to the properties of water and ice.[36,37,38] The bent shape gives it a dipole moment and determines how the molecules can fit together in a crystal. The difference in electronegativity between oxygen and hydrogen causes the electrons that are involved in the covalent bonds to be more attracted to the O atom. As a consequence, the H-O covalent bonds are highly polar. Since the two polar covalent bonds do not lie in a straight line, the water molecule as a whole is polar. The consequent charge displacement gives rise to an electric dipole

moment, oriented along the bisector of the H-O-H angle with its positive end on the hydrogen side of the molecule. *Figures 4.6a,b,c,d,e* summarize the discussed properties of a water molecule. The non uniform charge distribution of a water molecule is shown in *figure 4.6f* through a gradation in color from green to purple.

One of the properties of polar molecules is the tendency to align themselves along the direction of an applied electric field. In liquid water, the dielectric constant is dominated by the reorientation of the molecules due to their large dipole moments. The resulting value is large. The high dielectric constant is the reason why water is an excellent solvent for ionic and covalent substances. In ice, the reorientation of molecules is more limited than in the liquid phase; in this case, the proton motion is mainly responsible for the large value of the dielectric constant.[43,44] The value of the dielectric constant of liquid water is 87.9 at 0°C; it increases on conversion to ice and increases further as the ice is cooled. For ice Ih, it is 99 at -20°C, and 171 at -120°C.[54] On heating, the dielectric constant drops, and liquid water becomes far less polar; it goes from 87.9 at 0°C, to 55.6 at 100°C.[43] In a similar fashion, the dielectric constant reduces if the hydrogen bonding is broken, for example because of the presence of a strong electric field. Pressure, on the other hand, increases the dielectric constant (which becomes 101.42 at 0°C and 500 MPa), due to its effect on the density.

Since H_2O is highly polar, it interacts with other polar molecules. Importantly, H_2O molecules are able to attract other H_2O molecules through a weak electrostatic interaction, the hydrogen bonding. This attraction is very sensitive to orientation, assuming a maximum value when the O-H-O atoms are lined up. The hydrogen bond in water holds the key to its structure and properties. Its strength is ~3 kcal/mole, much smaller than the strength of the covalent bond (~100 kcal/mole). The dynamic motion of atoms induces the hydrogen bonds to constantly break and reform. The result is a statistical distribution of different coordination numbers.

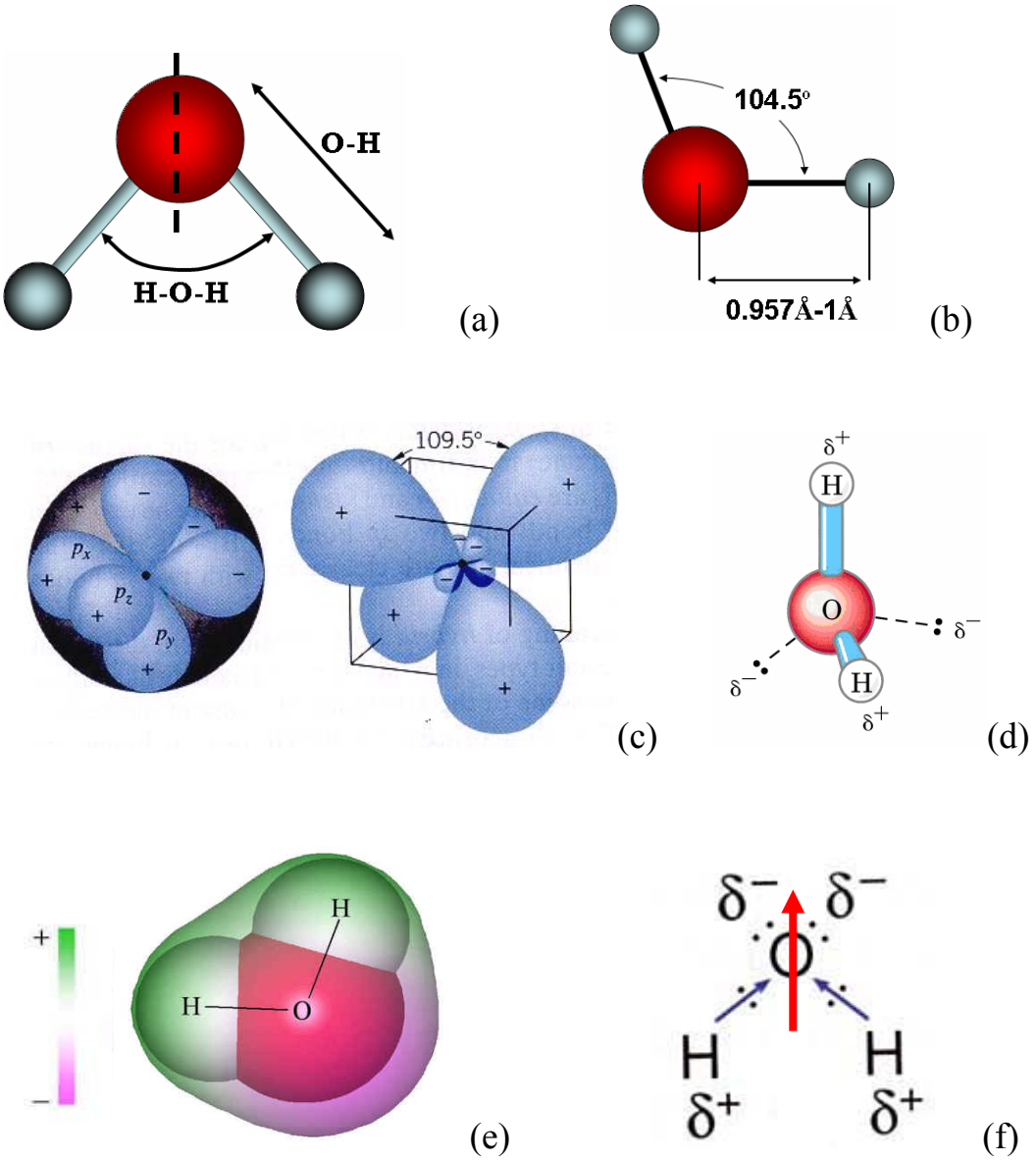

Figure 4.6: Properties of water. **(a)** Geometry of a free water molecule. The symmetry is C_{2v}, meaning that it has 2 mirror planes and a C_2 axis. **(b)** In liquid water, we can assume with good approximation that the bonding angle H-O-H is 104.5° and that the bonding length O-H is ~1 Å. **(c)** The value of the H-O-H angle is close to the angle expected for sp_3 hybridization; however, an ideal tetrahedral structure should give an H-O-H bond angle of 109.5°. **(d)** Since the lone pairs repel each other more than the O-H bonds, the covalent bonds are pushed closer, making the H-O-H angle less than 109.5°. **(e)** The non uniform charge distribution around O is illustrated through the use of a color gradient (green=positive, purple=negative). **(f)** The dipole moment of a water molecule is represented by a red arrow.

Due to the fact that each H_2O molecule can form hydrogen bonds with other H_2O molecules, an elaborate inter-molecular network gives rise to the different crystallographic phases of water. The most common form of ice is ice Ih; it is, in fact, the form of all natural snow and ice on Earth. Ice Ih has hexagonal symmetry and space group $P6_3/mmc$.[43] In this form of ice, a water molecule forms hydrogen-bonds with four surrounding molecules. Two of these are hydrogen-bonded to the O atom of the central H_2O molecule, while each of the two hydrogen atoms is bonded to another neighboring H_2O molecule. The four bonds from each O atom point toward the four corners of a tetrahedron centered on the O atom. In ice Ih, these bond angles are nearly the same as the perfect tetrahedral angle (109.5º). This basic assembly repeats itself in three dimensions to build the ice crystal.[38]

In *figure 4.7*, a comparison between a three-dimensional local structure of ice Ih and liquid water is shown. The greater openness of the ice structure is necessary to ensure the strongest degree of hydrogen bonding in the crystal lattice.

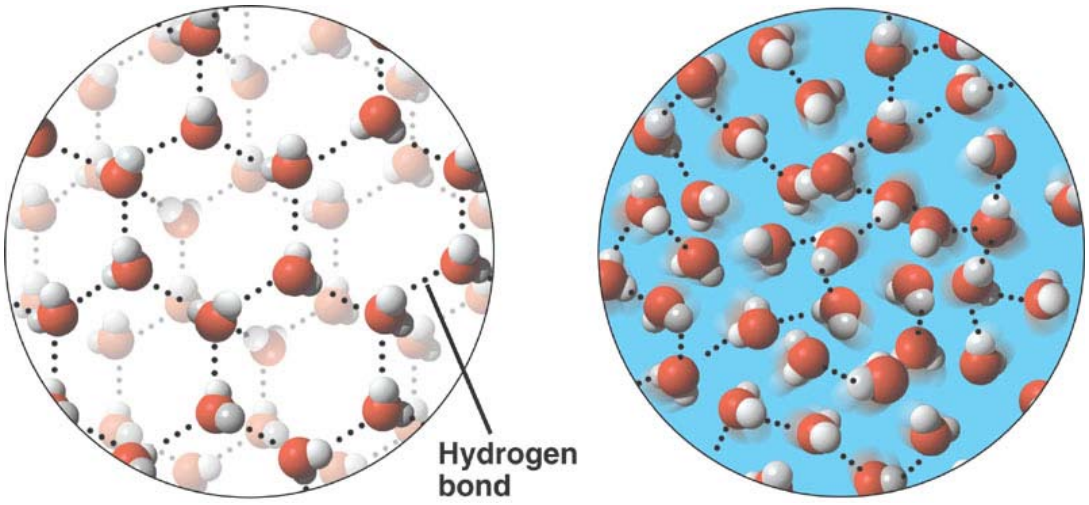

Figure 4.7: Hydrogen-bonds in ice Ih (left) and liquid water (right). H-bonds in ice give rise to a more stable structure.

In this work, the calculated pair distribution function (PDF) of ice was based on the ordered form of ice Ih, i.e. ice XI. This type of ice represents the low-temperature equilibrium structure of hexagonal ice. The transition ice Ih→ice XI is usually induced by doping ice Ih with alkali hydroxides below a temperature of 72 K (below 76 K in D_2O). So far, the most effective dopant has been KOH. The hydroxide ions create defects in the hexagonal ice allowing protons to jump more freely between the oxygen atoms. As a result, ice XI is a proton-ordered form of the hexagonal ice, forming crystals with orthorhombic symmetry (space group $Cmc2_1$). The described structure is shown in *figure 4.8*; the unit cell has dimensions a=4.5019 Å, b=7.7978 Å, c=7.3280 Å (90º, 90º, 90º).[43]

4.3.1 Molecular vibration of water

A free water molecule has three normal modes of vibration, two stretching modes (the symmetric stretching mode ν_1, and the asymmetric stretching mode ν_3) and one bending mode ν_2 (*figure 4.9*). The absorption frequencies v_3 and v_1 depend on the force necessary to stretch the covalent O-H bond, while the bending mode v_2 depends on the force necessary to change the bond angle. The dipole moments change in the direction of the movement of the oxygen atoms, as shown by the arrows in *figure 4.9*. The three frequencies have approximately the following values:[43]

ν_1=450 meV ν_2=200 meV ν_3=465 meV

In liquid water and ice, the infrared and Raman spectra are far more complex than in the vapor phase due to vibrational overtones and combinations with librations. Librations are due to the restrictions imposed by hydrogen bonding. They depend on the momenta of inertia of the molecule. For instance, the fact that D_2O has momentum of inertia that are almost double the ones of H_2O reduces the frequencies by a factor of $\sim\sqrt{2}$.

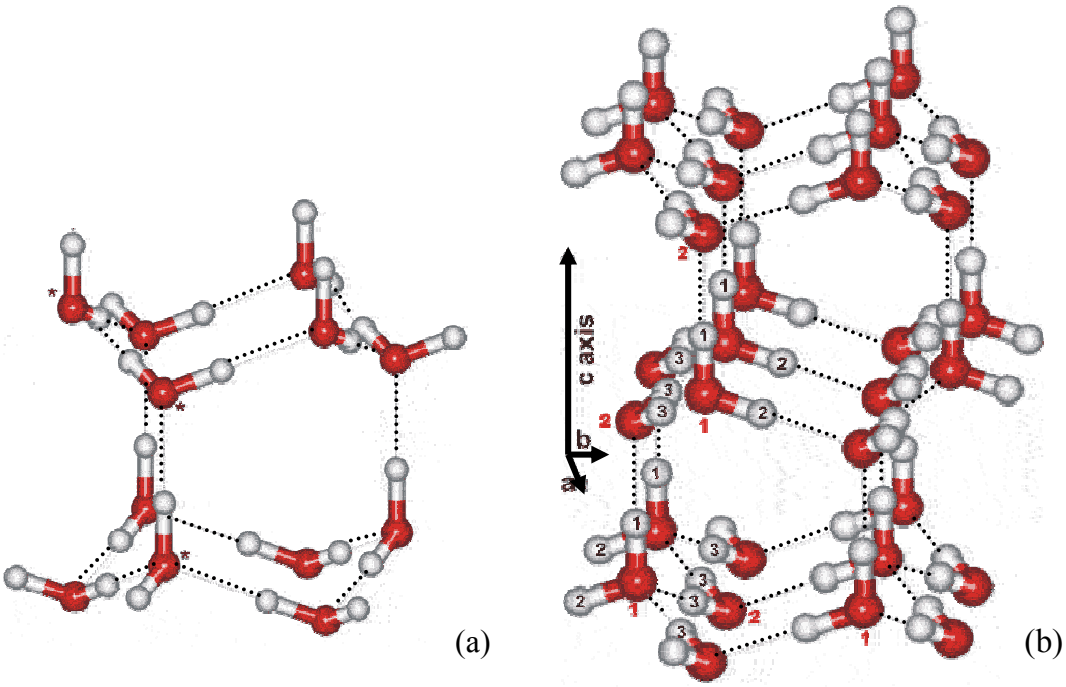

Figure 4.8: Structure of ice. **(a)** Ice Ih, the hexagonal ice with space group $P6_3/mmc$; it is the form of all natural snow and ice on Earth. **(b)** Ice XI, the low temperature proton-ordered structure of ice Ih. It has orthorhombic symmetry (space group $Cmc2_1$). The transformation process from ice Ih→ice XI requires dopant defects and a temperature < 72K.

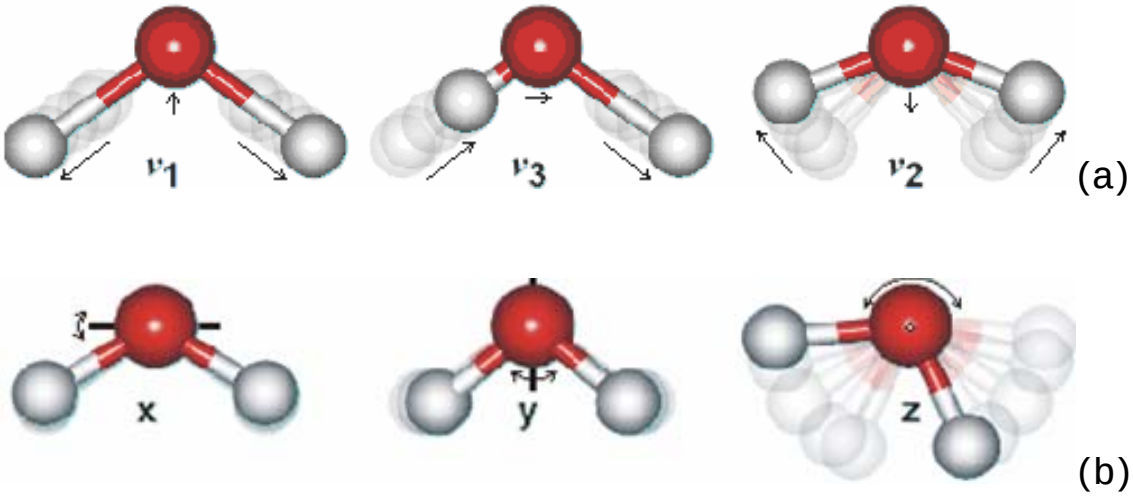

Figure 4.9: Vibration modes of water. **(a)** The three normal modes of vibration of a free water molecule: ν_1 is the symmetric stretching mode, ν_3 is the asymmetric stretching mode, and ν_2 is the bending mode. **(b)** Librations. In liquid water and ice, things get more complicated due to the possible combinations of the normal modes with librations. Librations depend on the momentum of inertia of the molecule along x, y, and z.

4.3.2 Self-ionization of water

Water is not a simple collection of H_2O molecules. Self-ionization always occurs: one water molecule donates a proton, and another one accepts the proton. The ionization reaction is reversible and it can be written as follows:

$$2H_2O \rightarrow H_3O^+ + OH^-$$

Due to this process there is always at least a small concentration of both H_3O^+ and OH^-. Because of the presence of these ions, water is not a perfect insulator. However, since the concentrations of H_3O^+ and OH^- are small, water is not a good conductor either. The concentrations of the two ions in pure water are the same and equal to 1.0×10^{-7} M. The **7** in the power of this number gives the characteristic pH=7 of neutral water.

4.4 Sample preparation

The superconducting cobaltate sample was prepared at Oak Ridge National Laboratory (ORNL) by intercalating D_2O molecules into Na-deficient Na_xCoO_2. $Na_{0.75}CoO_2$ powder was placed in a 6.6molar Br_2/CH_3CN solution for 2-5 days. After carefully filtering and washing in pure CH_3CN and CH_3CN/D_2O, the sample was further deuterated by stirring in the distilled D_2O. The detailed description of the procedure can be found elsewhere.[2] The estimated stoichiometry of the superconducting sample was $Na_{0.35}CoO_2 1.4D_2O$, and T_C was 4.5 K. The resulting sample was pure in D_2O. The choice of heavy water over regular water was made in order to avoid the disturbing background due to inelastic scattering from H.

Chapter 5

Experimental analysis and results

In this chapter, the study of $Na_{0.35}CoO_2 1.4D_2O$ at two different temperatures, T=15 K and T=100 K, is presented. Powder neutron diffraction data were analyzed using the Pair Distribution Function (PDF) technique. The measured and calculated PDFs of $Na_{0.7}CoO_2$, $Na_{o.35}CoO_2 1.4D_2O$, and D_2O were compared. In order to determine any local structural change within the intercalated water molecules, the analysis has been concentrated in the intra-molecular range of D_2O (<1.7 Å). The possible implications of this work are discussed at the end of the chapter in terms of electron conduction and superconductivity.

5.1 Data collection and analysis

The neutron diffraction experiments discussed in this thesis were performed at the NPDF diffractometer at the Los Alamos Lujan center (see *paragraph 3.7.1*). Data were collected at a temperature of 12 K in the case of heavy water and at two different temperatures, T_1=15 K and T_2=100 K, in the case of sodium cobaltate. About 4 grams of each sample, sealed in a vanadium can, were used. The cutoff value of Q (i.e. Q_{max}) was chosen to be 42 Å (see *paragraph 3.8.4*). The data analysis was performed using the software PDFgetN.[27] This program obtains the total scattering structural function S(Q) and the pair distribution function G(r) from time of flight neutron powder diffraction data. Once all the information about the sample, the instrument and the detector banks is entered, there are three main steps that lead to the PDF. First of all, the measured data are corrected for background scattering, container scattering, and incident spectrum

according to the following equation:

$$I = \frac{(S - S_B) - \alpha(C - C_B)}{V - V_B}$$

S represents the sample scattering, *C* the scattering from an empty sample container, and *V* the scattering from a vanadium sample, which gives a characterization of the incident spectrum. The subscript 'B' indicates the background spectra for S, V and B. The factor α takes into account the absorption of the sample. Therefore, a PDF measurement usually requires three characterization runs before the sample measurement can be performed: vanadium, empty container, and instrument background.

In a second step, absorption, multiple scattering, and the Plazcek inelastic correction can be taken into account. The normalized intensities from the different detector banks are combined together to give the final S(Q). One of the most important requirements in a PDF analysis is to get a properly normalized S(Q). The goal is to normalize S(Q) to one when values of Q are high (*figure 5.1*). The quantity that controls the normalization of *S*(*Q*) is the effective sample density. As a general rule, when the effective density increases, the asymptote of S(Q) decreases and vice versa. In many cases, the effective sample density is the only parameter that is necessary to adjust to get a good PDF. The normalization of S(Q) can be done either manually, by adjusting its asymptotic behavior, or automatically, letting the program determine the best effective density value. Once a correctly normalized S(Q) has been obtained, G(r) can be calculated according to its definition.

Figure 5.2 shows the reduced structural function Q[S(Q)-1], which is the quantity that is directly used to Fourier transform the data. Since S(Q)→1 at high Q, Q[S(Q)-1] oscillates around zero at high Q. *Figure 5.3* details the resulting pair distribution function G(r).

All of the following three figures (*5.2, 5.3,* and *5.4*) show the output of PDFgetN in the case of the deuterated sodium cobaltate $Na_{0.35}CoO_2yD_2O$. The graphs are obtained directly from PDFgetN using the plotting program KUPLOT.[27]

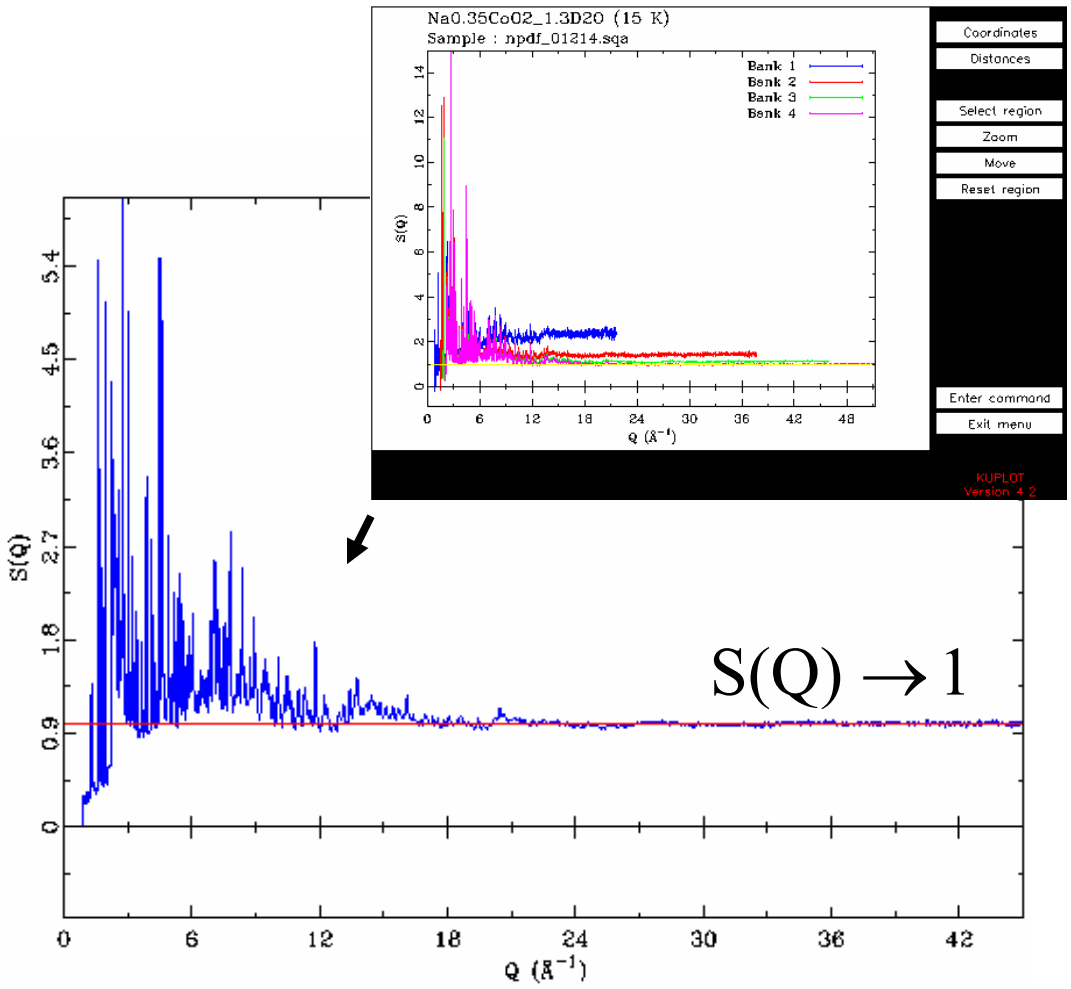

Figure 5.1 The values of S(Q) calculated for each different bank are blended together to obtain a single final structural function S(Q). A correctly normalized S(Q) converges at one for large Q. Data refers to $Na_{0.35}CoO_2yD_2O$.

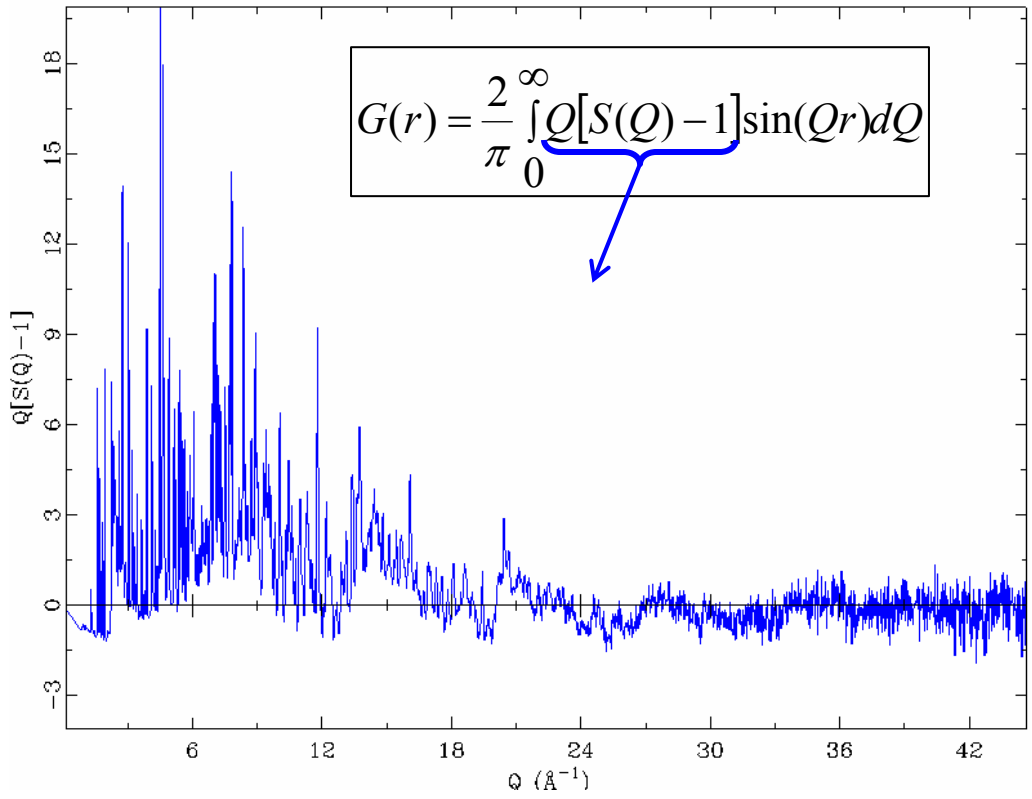

Figure 5.2: The total scattering structural function S(Q) can be plotted in the form of the reduced structural function Q[S(Q)-1]. Since S(Q) approaches one as Q increases, Q[S(Q)-1] oscillates around zero at high Q. This is the function directly used when data are Fourier transformed into G(r), as the formula in the inset indicates. Data refers to $Na_{0.35}CoO_2yD_2O$.

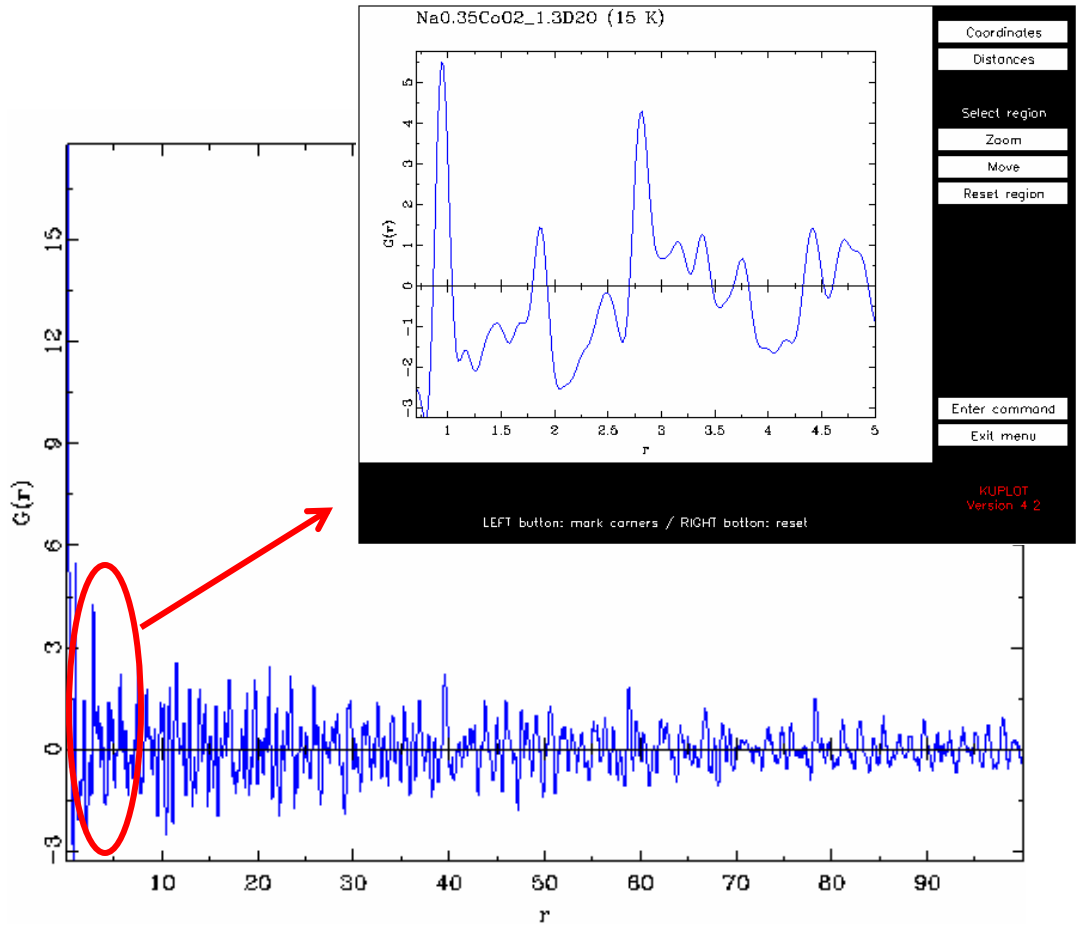

Figure 5.3: The pair distribution function G(r) of $Na_{0.35}CoO_2yD_2O$, obtained from PDFgetN and plotted with KUPLOT. G(r) oscillates around zero at high Q. Each peak corresponds to the distance in Å between two atoms. The insert shows the graphical interface of PDFgetN for G(r) in the range from 0 Å to 5 Å.

5.2 Experimental pair distribution functions

The experimental pair distribution function G(r) of $Na_{0.35}CoO_2 1.4D_2O$ is shown in *figure 5.4* for both temperatures, T_1=15 K and T_2=100 K. The first very sharp peak is a spurious peak that does not correspond to any real atom-atom correlation. There is no significant difference between the two curves. Therefore, for the sake of simplicity, only one set of data will be considered in the following discussion - the one at 15 K. The conclusions will, then, apply to both temperatures. The range in the figure has been limited to 5 Å for a more detailed characterization of the peaks.

In *figure 5.4b*, the baseline for G(r) has been included; it is the red line that starts from zero. At low values of r, in fact, G(r) is a straight line that goes through zero; the slope of this line is proportional to the average density ρ_0 of the sample, that is $G(r) = -4\pi\rho_0 r$ for $r \to 0$. When calculating ρ(r) from the data, a theoretical value of the average density is assumed, according to the definition $\rho(r) = \rho_0 g(r)$. This value determines the baseline.

However, if we want to take into account the weight of each peak, it is more convenient to plot the data in terms of the radial distribution function $R(r) = 4\pi r^2 \rho(r)$ instead of G(r). In this situation, in fact, the natural baseline is zero since $\rho(r)$ goes to zero as $r \to 0$. For this reason, we will use the RDF later on in our analysis. *Figure 5.5* shows a comparison between the baseline for G(r) and R(r) in the case of $Na_{0.35}CoO_2 1.4D_2O$; a narrow range from 0.8 Å to 2 Å has been chosen to enhance the difference.

The pair distribution functions of D_2O and $Na_{0.7}CoO_2$ are shown in *figure 5.6*. In both PDFs, several peaks are visible. As for water, according to literature, the sharp peak at ~1 Å should correspond to the O-D distance, while the less sharp peak at 1.6 Å to the D-D distance. These two distances are the intra-molecular distances expected within a free water molecule. As for $Na_{0.7}CoO_2$, no peaks appear to be in our range of interest, below 1.7 Å. In order to verify these assumptions for D_2O and $Na_{0.7}CoO_2$, and in order to find out what distance-correlation each peak in the experimental PDF of $Na_{0.35}CoO_2 1.4D_2O$ represents, the calculated PDFs have been considered.

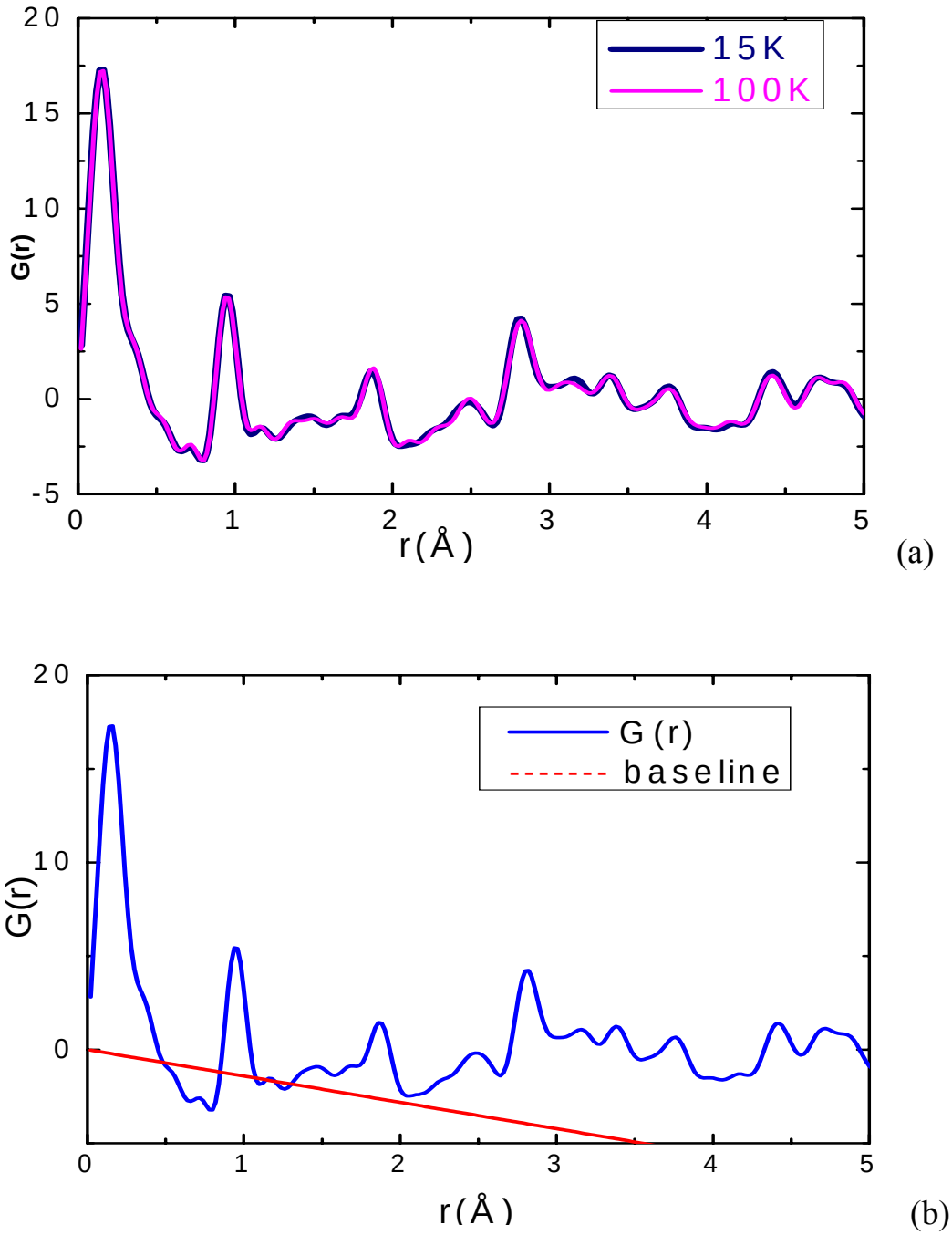

Figure 5.4: (a) G(r) of $Na_{0.35}CoO_2 1.4D_2O$ at two different temperatures T=15 K, 100 K. No significant difference is visible at low r. **(b)** The baseline for G(r) has been included for the set of data at 15 K. The first very sharp peak is a spurious peak and does not correspond to any real distance-correlation; it will not be considered in further analysis.

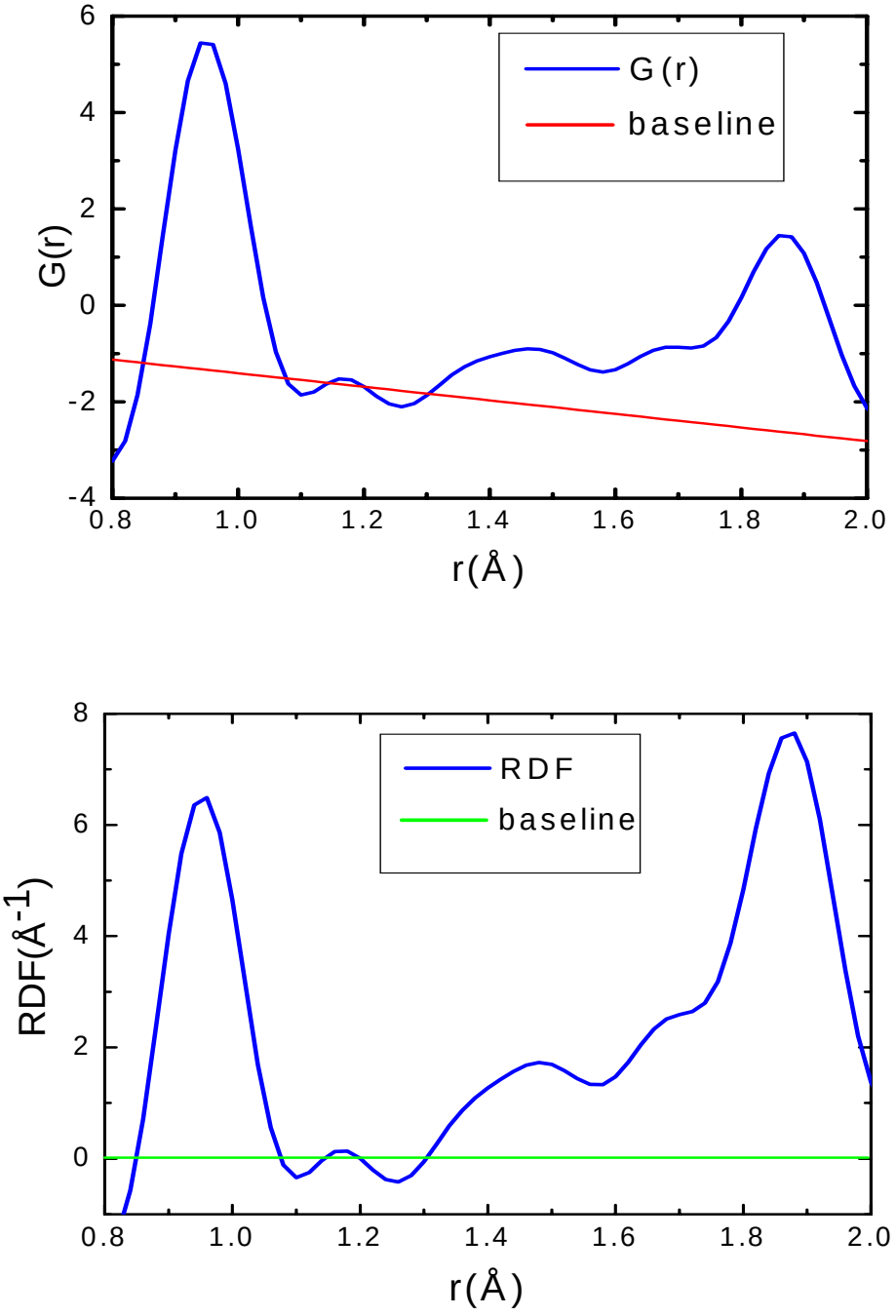

Figure 5.5: Comparison between the baseline for G(r) and for R(r) in the case of $Na_{0.35}CoO_2 1.4D_2O$. When r $\rightarrow$0, G(r)$=-4\pi\rho_0 r$; on the other hand, when r $\rightarrow$0, $\rho(r)$ goes to zero, and so does R(r). The range from 0.8 Å to 2 Å has been chosen here because it is the one that will be considered later in our analysis.

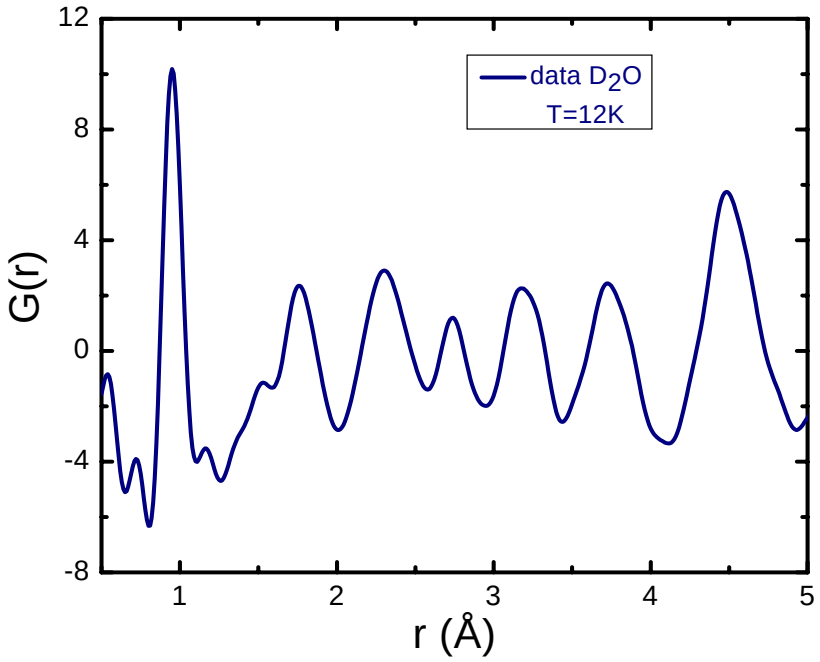

(a)

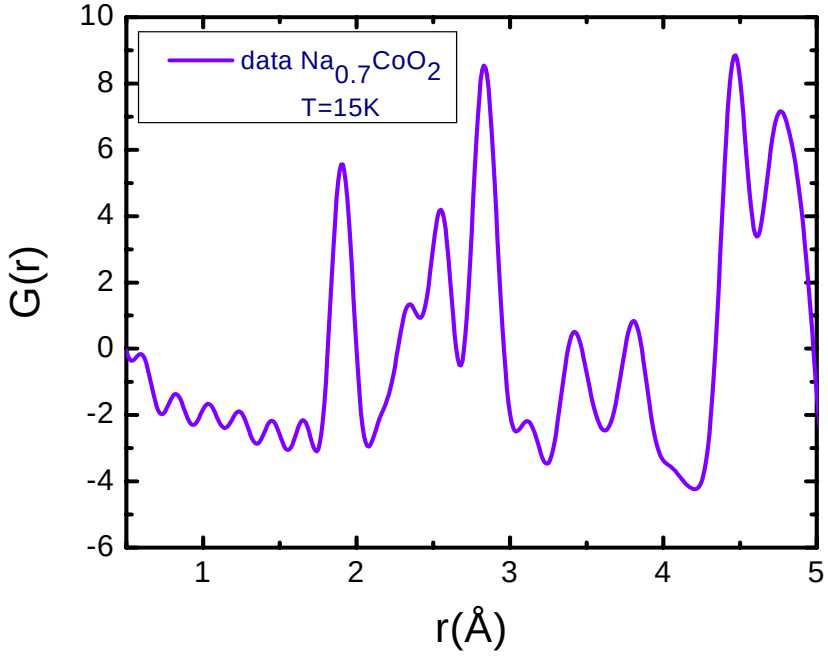

(b)

Figure 5.6: **(a)** Experimental PDF of heavy water. According to literature, the first peak at ~1Å corresponds to the O-D correlation, while the second less sharp peak at ~1.6 Å to the D-D correlation within a single D_2O molecule. **(b)** Experimental PDF of $Na_{0.7}CoO_2$. The most important piece of information we can extract from this figure is that no peaks appear to be below 1.7 Å.

5.3 Calculated pair distribution functions

Since D_2O and $Na_{0.7}CoO_2$ are the two compounds that give rise to the superconducting phase, it comes naturally to first analyze each of them separately and then, combine the results in terms of $Na_{0.35}CoO_2 1.4D_2O$. We are interested in the intra-molecular range, so we need to associate each peak that falls in that range with a specific atom-atom distance. The calculated partial PDF gives the distances between species of atoms and, therefore, represents the ideal tool to identify each peak. In the case of water, we will have the three distances D-D, D-O, and O-O; in the case of $Na_{0.7}CoO_2$, we will have the distances Na-Na, Na-Co, Na-O, Co-Co, O-O, and Co-O. The calculated PDF of (heavy) water is based on the structure of low temperature ice (see chapter 4). The PDF of $Na_{0.7}CoO_2$ was calculated using the structural parameters obtained using Rietveld refinement and the super-cell proposed by Jorgensen (see *chapter 4*).[5]

The partial pair distribution functions of heavy water and $Na_{0.7}CoO_2$ are shown in *figure 5.7*. In D_2O, the first two calculated peaks are found at 0.97 Å and 1.58 Å; they correspond indeed to the D-O and D-D distances, as expected. In the case of $Na_{0.7}CoO_2$, there are no peaks below 1.8 Å. The first sharp peak appears at 1.9 Å and corresponds to the Co-O distance. We can conclude that, in the distance range from zero to 1.8 Å, the dry cobaltate $Na_{0.7}CoO_2$ brings no contribution to the peaks observed in the diffraction spectrum of $Na_{0.35}CoO_2 1.4D_2O$.

5.4 Results

In the previous paragraph, we determined that no peaks belonging to $Na_{0.7}CoO_2$ can be found below 1.7 Å. Thus, we expect that all the peaks observed in $Na_{0.35}CoO_2 1.4D_2O$ below 1.7 Å are due to the presence of D_2O. A good way to verify this supposition is to make a comparison between the measured spectrum of heavy water and deuterated sodium cobaltate. As already mentioned, we are interested in studying the changes in the local structure within an inserted D_2O molecule. For this reason, in the following analysis

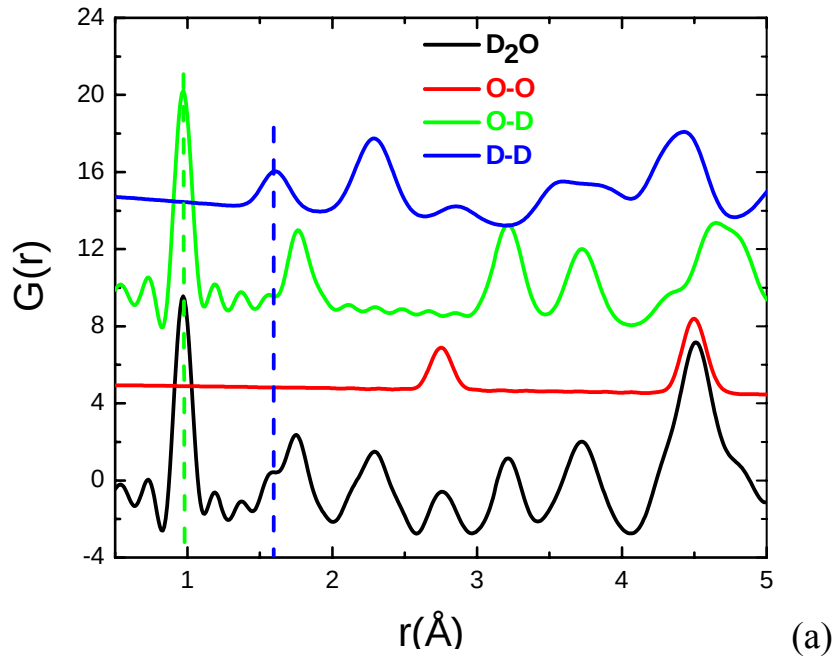

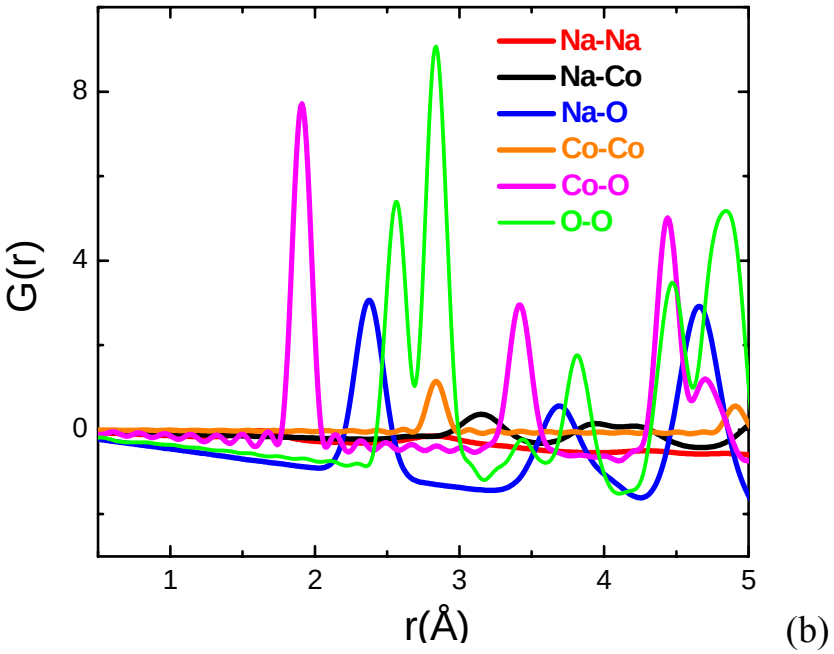

Figure 5.7: **(a)** Calculated partial PDF of heavy water; **(b)** calculated partial PDF of $Na_{0.7}CoO_2$. In water, the first two peaks correspond to the D-O (0.97 Å, green dotted line) and D-D (1.58 Å, blue dotted line) distances. In dry sodium cobaltate, there are no peaks below 1.7 Å; we can conclude that all the peaks that appear below 1.7 Å in the experimental spectrum of the deuterated cobaltate are only due to D_2O.

the r-range has been narrowed to just a few Å. *Figure 5.8* shows a comparison between the experimental G(r) of $Na_{0.35}CoO_2 1.4D_2O$ and D_2O. The O-D peak in the experimental PDF of heavy water coincides exactly with the first sharp peak in the PDF of $Na_{0.35}CoO_2 1.4D_2O$. In other words, the peak that appears at 0.95 Å in the PDF of $Na_{0.35}CoO_2 1.4D_2O$ corresponds indeed to the distance between the O atom and the D atom within an inserted D_2O molecule.

In a similar fashion, knowing that the first D-D peak is located at r=1.53 Å in the experimental PDF of water, we expect to find in the PDF of $Na_{0.35}CoO_2 1.4D_2O$ a peak at about the same r. The surprise is that at 1.53 Å, there is no peak at all. Instead, two peaks are visible, one above and one below the expected D-D peak position.

In order to evaluate the positions of the two unknown D-D peaks, a Gaussian fit has been carried out in a short interval of distances that includes the peaks. Since, in this case, the weight of the peaks is of extreme importance, the RDF has been used. As a fitting constraint, the area of the Co-O peak at 1.87 Å has been maintained as the one expected from calculation. The fit results are shown in *figure 5.9*. The first D-D peak has been found to be centered at r_1=1.46 Å, while the second D-D peak has been found to be centered at r_2=1.68 Å. Since the O-D distance in $Na_{0.35}CoO_2 1.4D_2O$ corresponds to the expected O-D distance in D_2O, such a result suggests that the D-O-D bond angle of the inserted water molecules is altered. In fact, considering a fixed O-D distance of 0.95 Å and a double D-D distance of 1.46 Å and 1.68 Å, two bond angles are found; the D-O-D angle that corresponds to r_1 is 100º, the D-O-D angle that corresponds to r_2 is 124º. The situation is pictured in *figure 5.10*.

The bond angle in regular water and ice always assumes a value that goes from 104.5º in a free water molecule to 109.5º in hexagonal ice. Regardless of the crystallographic phase, the H_2O (or D_2O) molecules preserve their geometry with well defined O-H (or O-D) and H-H (or D-D) distances, and H-O-H (or D-O-D) bond angle. In the case of deuterated sodium cobaltate $Na_{0.35}CoO_2 1.4D_2O$, however, the situation is different. Our results show that at both temperatures, T_1=15 K and T_2=100 K, the D-D distance and the D-O-D angle are significantly different from those of ordinary water.

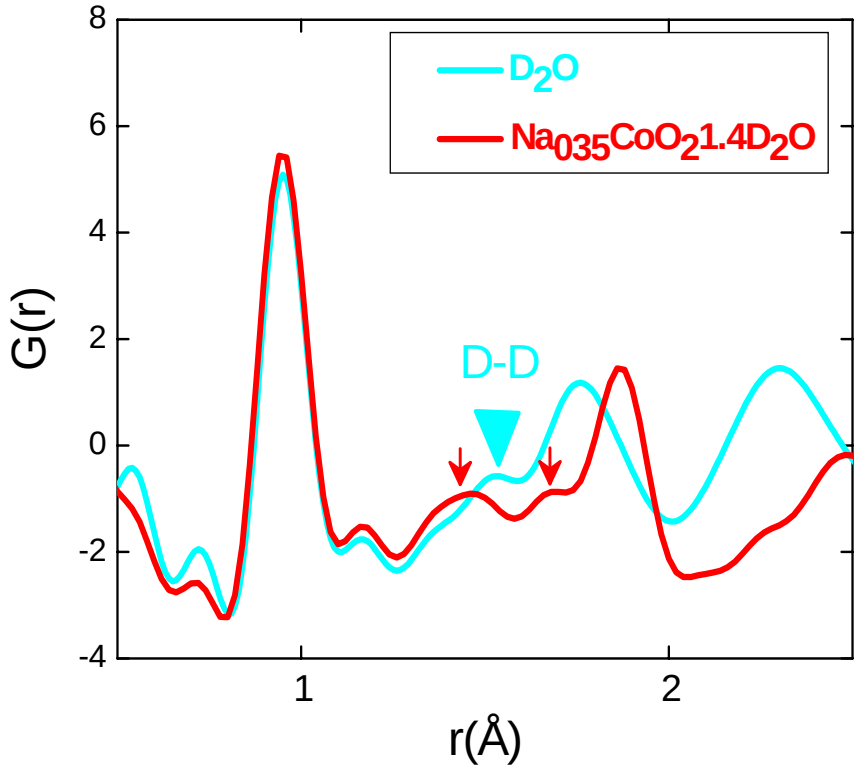

Figure 5.8: Comparison between the experimental pair distribution functions of heavy water and $Na_{0.35}CoO_21.4D_2O$. The peak that appears at 0.95 Å in both PDFs corresponds to the O-D peak. As for the D-D peak, in water it is found at r=1.52 Å, while in $Na_{0.35}CoO_21.4D_2O$ such a peak does not exist. Instead, two peaks appear, one above and one below r=1.52 Å.

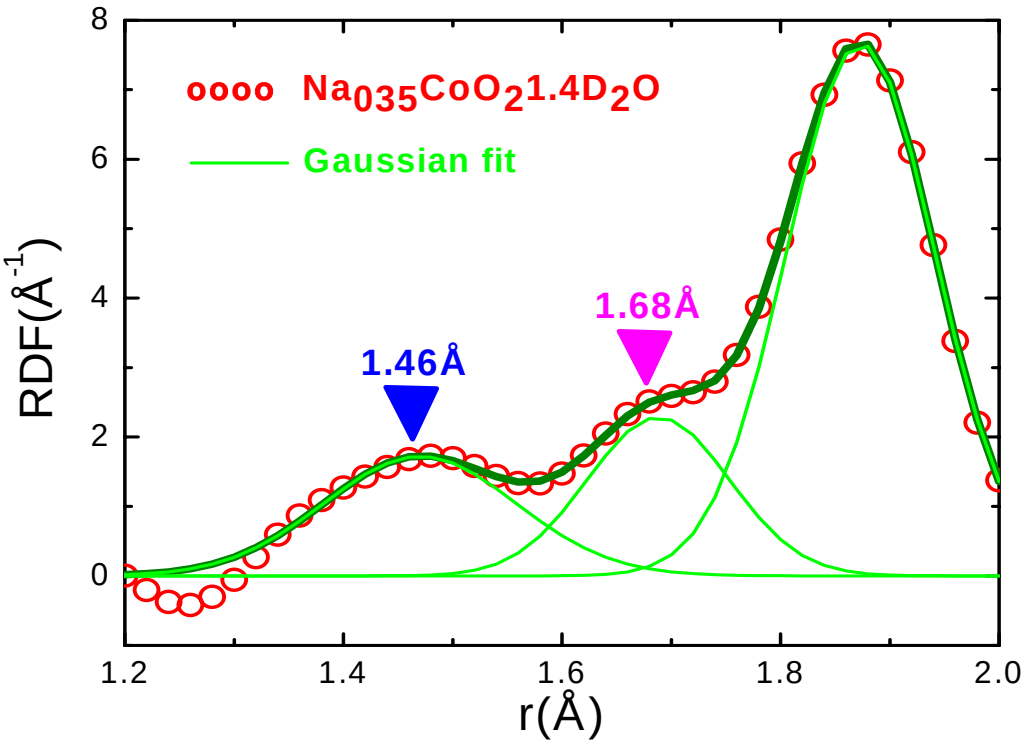

Figure 5.9: The Gaussian fit performed to evaluate the positions of the two unexpected D-D peaks. A constraint was applied to the area of the Co-O peak, located at 1.87Å. The result of the fit indicates that the first peak is centered at 1.46 Å, while the second one is centered at 1.68 Å.

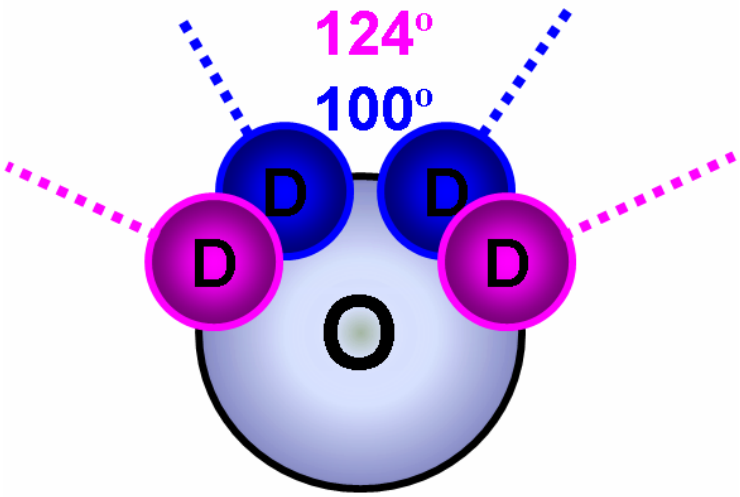

Figure 5.10: The new geometry of the inserted water molecules. Since the O-D peaks in $Na_{0.35}CoO_2 1.4D_2O$ and D_2O coincide, it is possible to estimate the two bond angles that correspond to the two D-D peaks found in $Na_{0.35}CoO_2 1.4D_2O$. The new geometry of the inserted water molecules is illustrated in the figure. The D-O-D angle that corresponds to r_1=1.46 Å is 100º; it is smaller than the expected bond angle of a regular water molecule. The D-O-D angle that corresponds to r_2=1.68 Å is 124º; in this second case, the angle is bigger than the one expected for a regular water molecule.

Two coexisting distributions of possible D-D distances arise. They translate into two distributions of possible D-O-D bond angles. In other words, when water is intercalated into the dry sodium cobaltate, its geometry is altered. Two populations of water molecules emerge; one has a smaller angle with respect to the D-O-D bond angle of regular water, while the other one has a larger angle. The question that naturally arises at this point is: do the modified water molecules in superconducting $Na_{0.35}CoO_2 1.4D_2O$ play a role in the electronic conduction?

5.5 Discussion of the results

Up to now, calculations of the electronic structure of the system, done by other research groups, largely neglected the importance of the role of water. Furthermore, in the analysis of experimental data, the structure of water has been always considered rigid.

No modifications of its geometry have been taken into account. Our results raise several questions on the real function of water within the structure of $Na_{0.35}CoO_2 1.4D_2O$. The structural modifications seen with the PDF suggest that water is not only a space separator between layers of cobalt and sodium. From our current data, it is unclear whether water contributes to the conduction of the system or not. Further neutron scattering experiments and theoretical calculations that take into account the possible implications of the modification of the water geometry are certainly needed. However, even with a partial knowledge of the structural and electronic properties of this compound, we can still discuss some possible scenarios.

At first glance, we can speculate that there are two possible roles of the intercalated water in sodium cobaltate:

1. One possibility is that the inserted water molecules simply re-arrange themselves within the sodium cobaltate structure, without any contribution to the overall electron conductivity of the final compound. In this case, strictly structural reasons would lead the water molecules to assume a broad distribution of different bond angles. Thus, what we see with the PDF is just a static order/disorder of the water molecules between two successive layers of CoO_2 and Na.

2. Another possibility is that, instead, water has a more active role in the electronic conduction of $Na_{0.35}CoO_2 1.4D_2O$. In this case, the 100º angle could be associated with the group of water molecules that slightly reduce their bond angle in order to be accommodated into the structure; on the other hand, the 124º angle could be associated with the group of water molecules that actively participate in the conduction mechanism.

Only the second hypothesis will be further examined here. Since, as of today, theoretical and experimental conclusions have been sometimes contradictory, the discussion will be conducted in two steps. First, we will consider how previous experimental results obtained by other groups could be related to ours. Second, at the end of the chapter, we will try to put all the experimental evidence together and discuss some possible scenarios that may include water as a contributor to electronic conduction and superconductivity.

5.5.1 Experimental evidence

Recently, Raman spectroscopy has been used to study the superconducting hydrated sodium cobaltate $Na_{0.3}CoO_2 1.4H_2O$. The results of the measurements suggest that H_3O^+ ions are present in the structure.[45] The conclusions were that, since the concentration of hydronium ions formed by the self-ionization of water is relatively small, it may be possible that the formation of the deuterated compound is accompanied by the insertion of additional H_3O^+. Other Raman measurements, however, did not confirm the same results. The debate on the H_3O^+ ions in $Na_{0.35}CoO_2 1.4H_2O$ is still open.

Ab-initio calculations show that the hydronium ion (H_3O^+) has a flattened pyramidal structure. For the gas phase, calculations give a value of 0.961 Å for the O-H bond length and a value of 114.7° for the H-O-H angle; in the liquid phase, these two values become 1.002 Å, and 106.7°, respectively.[46] Considering these calculated values of the H-O-H angles, the possibility that one of two the angles found in our deuterated sample is due to the hydronium ion should be taken into account.

In water, the large difference between the mass of hydrogen and the mass of oxygen leads to an ease of rotation, and to significant relative and constant motions of the H nuclei. If the D-D distance changes, the dynamics of the water molecule will change. While the libration mode is not affected by a change in the D-D distance, the bending mode certainly is. In the case of the smaller D-O-D angle (100º), the two D atoms become closer; hence, their interaction becomes stronger. As a consequence, the bending mode frequency should increase. On the other hand, in the case of the bigger D-O-D angle (124º), the water opens up and the interaction between the two D atoms becomes weaker. Therefore, the bending mode frequency should decrease.

For regular water and ice, the bending mode frequency is ~200 meV (see *chapter 4*). No additional modes between 150 meV and 200 meV have ever been reported.[47,48,49] According to our previous considerations, in $Na_{0.35}CoO_2 1.4D_2O$, one mode at a frequency higher and a frequency lower than 200 meV should appear. Since the phonon density of the states of the anhydrous cobaltate cuts at 100 meV, any additional mode in the range from 150 meV to 200 meV must be attributed to the inserted water molecules present in

the deuterated compound. Inelastic neutron scattering measurements[4] have shown indeed the presence of an additional mode at 176 meV, a frequency smaller than the 200 meV expected in regular water (*figure 5.11*).[3] In the case of deuterium, we expect such a mode to appear at ~128 meV, since it is the mass that determines the frequency of the bending mode. This mode would take into account the wider bond angle of 124º. Since the measurement was performed up to 250 meV, no evidence of the higher frequency mode, corresponding to the 100º angle, has been found so far.

Investigations on how changing the average cobalt oxidation state *n* affects the critical temperature T_C have been carried out.[36] A neutron powder diffraction experiment on a sample of $Na_xCoO_{2-\delta}4xD_2O$ (x~1/3) showed that structural modifications and lattice defects (as oxygen vacancies) may lead to a change in the value of *n* that would directly affect superconductivity. A critical temperature of 2.2 K was observed when *n*~3.6, while the maximum value of 4.5 K was observed when *n*~3.5. As the cobalt reduction T_C decreases and superconductivity rapidly disappears.

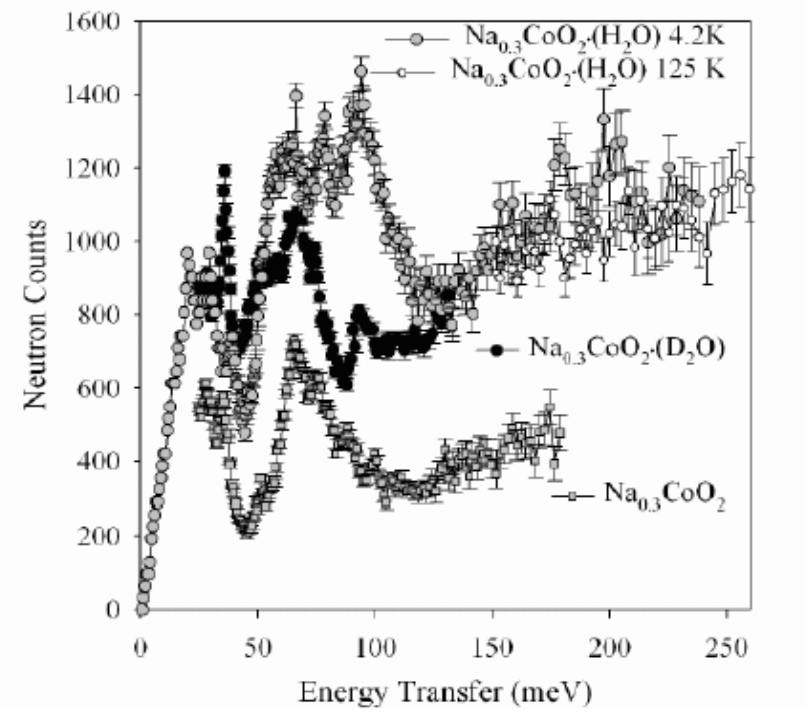

Figure 5.11: Phonon density of states for $Na_{0.3}CoO_2$, $Na_{0.3}CoO_2(H_2O)$, and $Na_{0.3}CoO_2(D_2O)$. $Na_{0.3}CoO_2$ has a high energy cutoff of ~100 meV. The lattice dynamics of the superconducting compound exhibits a mode at 176 meV not found in H_2O.

Again using neutron powder diffraction, the same group also studied the compressibility of $Na_xCoO_2 4xD_2O$ (x~1/3) over the pressure range of 0-0.6 GPa.[50] It has been found that pressure increases the thickness of CoO_2 layer (*figure 5.12*). This effect has been related to a pressure-induced increasing of the strength of the hydrogen bond between one O atom of the CoO_2 layer and one D atom of the heavy water molecules close to the CoO_2 layer. This may induce a charge-redistribution between the Co–O bond and the hydrogen bond, causing a change in the O-Co-O angle within the layer. In this way, the CoO_6 octahedra become less distorted. The redistribution of charge would lead to a reduction of the average cobalt oxidation state *n*. As they previously related *n* directly to superconductivity, pressure is also directly related to T_C. According to this research group, the cobalt oxidation state should be added to the Na and the D_2O contents to fully describe the superconducting properties of sodium cobaltate.

Ice exists in a variety of phases, but, in all cases, water molecules are held together by a network of hydrogen bonds. Molecules are believed to be oriented without any net polarization. The possible existence of a form of ice in which there is a polar order of the water molecules has been the subject of an intense debate that dates back to the 1920s. Recently a few experiments[51,52,53] have provided evidence that at least a partial ferroelectric alignment can be induced by interaction with a surface or by doping with impurities. In the first case, it has been proposed that the interaction of a film of ice with

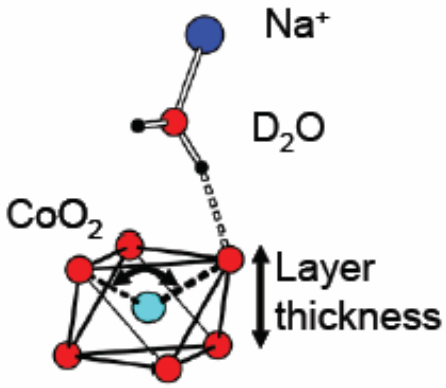

Figure 5.12: Effect of pressure on the CoO_2 layer. Pressure changes the thickness of the CoO_2 layer due to a redistribution of charge between the hydrogen bond D-O and the Co-O bond. As a consequence of this charge redistribution, the oxidation state of Co changes, thus directly relating pressure and the valence state of Co.

a substrate induces, first, a layer of molecules close to the surface to align; in a second step, these aligned molecules would influence a fraction of the remaining molecules to orient themselves as well. As a result, the sample would have a net polarization, which decays with the distance from the substrate. In the second case, it has been shown that doping hexagonal ice with hydroxide ions enhances the alignment. Below 72 K, this kind of doping gives rise to the ordered form of ice called ice XI (*chapter 4*). Results of neutron diffraction experiments on ice XI are consistent with a ferroelectric alignment of some water molecules, leading to the possible conclusion that ice XI is indeed ferroelectric. The exact degree of alignment, however, has not been completely determined.

One way that has been used to show that ice Ih exhibits a ferroelectric transition at low temperature or, in other words, to show that ice XI is ferroelectric, is to determine that the Curie-Weiss temperature T_0 is finite. The Curie-Weiss law, in fact, is:

$$\varepsilon_0 - \varepsilon_\infty = \frac{A}{T - T_0}$$

where ε_0 is the low frequency permittivity (up to ~10^3 Hz) of the orientation polarization, ε_∞ is the high frequency permittivity (from ~10^6 Hz to ~10^{14} Hz) of the orientation polarization, A is a constant, and T is the temperature. Therefore, the quantity $\varepsilon_0 - \varepsilon_\infty$ represents the amplitude of the orientation polarization. Several values of T_0 have been reported so far. In *figure 5.13a* the low frequency permittivity as a function of temperature is shown; these values of ε_0, and ε_∞=3.2, have been used to determine the Curie-Weiss plot of *figure 5.13b*. In this case, the extrapolated value of T_0 is ~2 K.[54]

5.5.2 Possible scenarios

As of today, there is no unique scenario that can be deduced by the experimental data available on sodium cobaltate. Many factors may contribute to trigger the superconducting state when sodium is removed and water is intercalated.

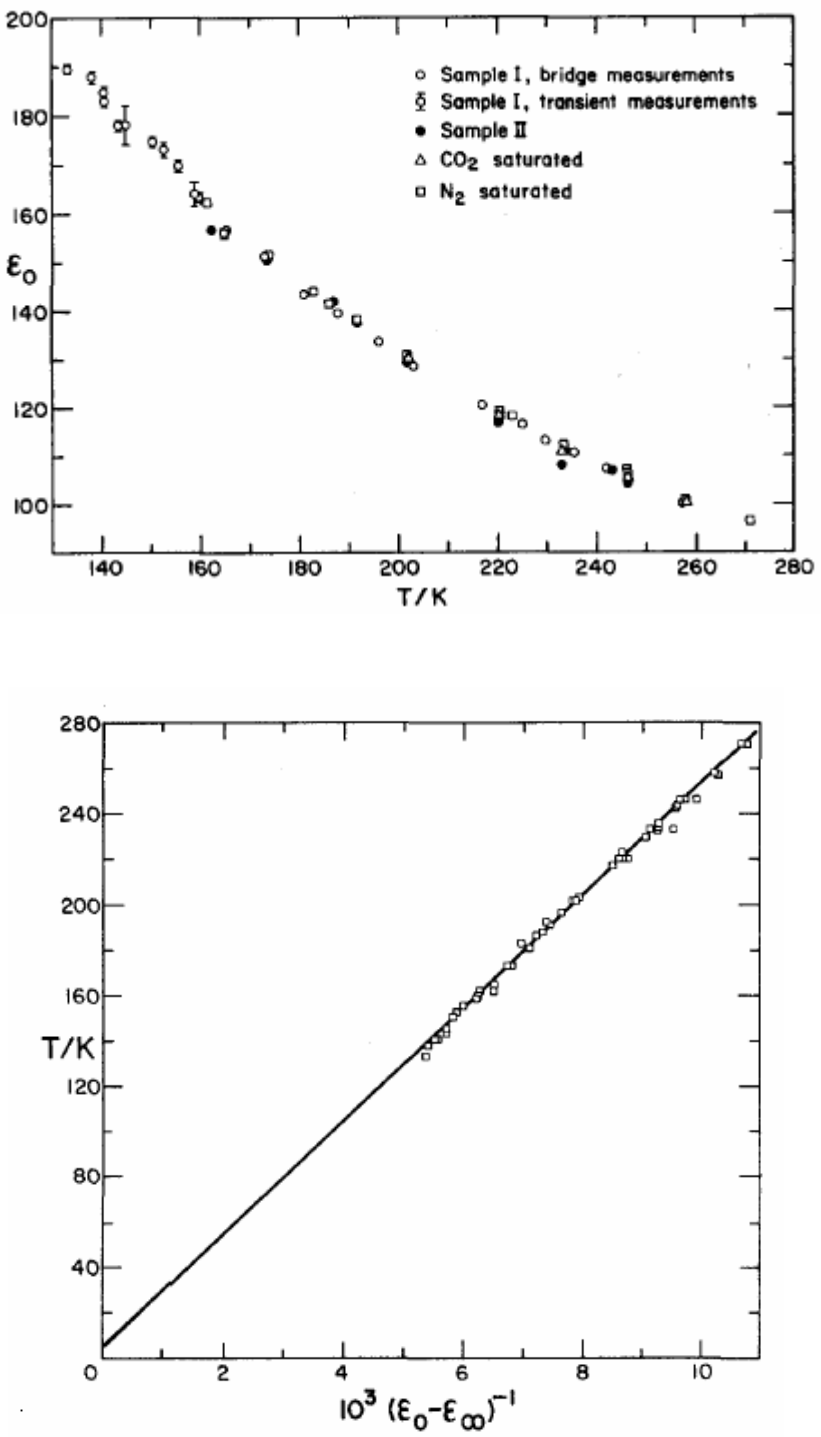

Figure 5.13: **(a)** Low frequency permittivity (ε_0) as a function of temperature (T) in ice. **(b)** Curie-Weiss plot. The quantity $\varepsilon_0 - \varepsilon_\infty$ is the amplitude of the orientation polarization. The Curie-Weiss temperature does not differ largely from zero and is ~2 K.

In nature, there are several examples of water-intercalated compounds where the geometry of the water molecule is altered; for example, the hydrous copper sulfate, in which water molecules with different bond lengths are found, and many hydrous minerals of the Earth's crust, in which the expansion of the H-O-H bond angle is clearly visible by means of neutron scattering. What makes the case of the hydrogenated (or deuterated) sodium cobaltate special is the possibility that, here, water could be an active ingredient in the electronic conduction process.

When considering the distribution of smaller bond angles, the first notable thing is that there are only a few degrees of difference from the bond angles of regular water/ice. The most likely scenario is that, in this case, water molecules simply change slightly their geometry to be accommodated into the new structure. In this picture, one of the two populations of water molecules would act as a space filler and separator, leaving the electronic active role to the one that undergoes the bigger structural modification.

Opening the bond angle up to 124° requires a conspicuous amount of energy. The bonding and non-bonding electron regions, in fact, become closer, and the electron-electron repulsion between them increases. This high energy cost in broadening the angle suggests that water may be embedded in an electronically active environment. Any change in the electron density within the lone pairs can result in a drastic change of the H-O-H angle. In particular, a reduction of the electronic density would cause a broadening of the angle.

As we already pointed out, self ionization is a process that naturally occurs in water due to its polar nature. In the case of sodium cobaltate, however, an additional induced ionization of water might also be considered. The fact that the cobalt and sodium layers result in having opposite net charge gives rise to an electric field between them. Since the activation barrier of ionization is relatively small, this field could induce an ion dissociation in water. The total concentration of the hydronium and hydroxide ions would then increase. In this scenario, water would be ionized and electronically active.

When subjected to an electric field, some molecules in the ice structure can rotate slightly without causing any bond to rearrange and the bond angle can distort to a small extent. This could be related to the smaller angle geometry observed with the PDF.

According to calculations, the H-O-H angle in H_3O^+ is larger than the regular bond angle found in water/ice. The wider angle geometry could then be related to the hydronium ions.

The presence of hydronium ions has been suggested by Raman measurements. Their presence would certainly influence the vibrational modes of water, especially the bending mode. In this frame, the observation of an additional bending mode at 176 meV would provide additional support to this hypothesis.

In ice, electronic properties arise from the flow of protons though the lattice. Proton motion along the ice structure occurs very easily, since only a few defects in the ice structure are able to induce this motion. The effect of this motion is that of reorienting the molecules along the path. The possible defects in the ice structure fall in two categories, the Bjerrum defects and the ionic defects. The first category includes empty bonds and bonds with two protons; the second category includes H_3O^+ and OH^-, which are formed by the transfer of a proton from one water molecule to the neighboring one, and are separated by jumps of protons from one end of a hydrogen bond to the other. However, in ice, ions do not move as complete entities. The O atom cannot move from one site to another; it is the motion of a proton along a bond that transfers the state of ionization from one molecule to another. Shifting a proton along the hydrogen bond requires ~0.5V/Å. The proton motion and the ion dissociation induced by the field between the layers imply a charge transfer. In our case, it would be possible to accumulate charge on the cobalt layer.

The interaction of water with the Co layer has been the object of a past neutron diffraction study. The Co oxidation state has been found to change when charge is redistributed between the O-H and the Co-O bonds. However, in this work, water has been maintained with a fixed rigid structure. If, instead, we add the possibility of a water modification, a more complex scenario could arise. We may assume that the alteration of the water molecules is due to an interaction with the Co layer.

An important role in the system may be played by phonons, vibrations of charged ions in a lattice. The displacement of the ions from their equilibrium positions creates a net electric potential felt by electrons zipping through the lattice. In our case, even only

considering the self ionization of water, OH^- ions could find themselves close to the Co layer and could interact with the holes vibrating in the layer. Electron-phonon coupling would be enhanced. A large electron phonon constant would give the glue for the formation of Cooper pairs. Superconductivity may set in.

Furthermore, experimental evidence of ferroelectricity in low temperature ice leads to the possible speculation that ice in this compound is electronically active. The high dielectric response of water when ice is cooled down may enhance the electron-phonon coupling and, in this way, set in the superconducting phase.

To complicate things, possible effects of the pressure exerted on the water molecules squeezed between the two layers of cobalt and sodium should be considered. It is well known that the phase diagram of ice depends on pressure. One possibility is that, locally, ice changes its phase. As a consequence, the bond angles would change. Pressure may change both the O-D-O and the O-Co-O angles. Pressure on ice has also the ability to increase the dielectric constant. Once again, the dielectric response of water could lead to superconductivity.

5.6 Conclusions

Our results show that the D-D distance and the D-O-D angle in $Na_{0.35}CoO_2 1.4D_2O$ are significantly different from those of ordinary water. Two coexisting distributions of possible D-O-D bond angles are observed. We speculate that the altered geometry of the intercalated water molecules is due to a modification of the dynamics of the hydrogen bond. Water could be ionized and electronically active. Because of recent experimental evidence of ferroelectricity in very low temperature ice, we speculate that, in this system, ice is active. One possible conclusion is that the strong dielectric response of water may enhance the electron-phonon coupling; in this case, water may play a key role in the superconductivity of $Na_{0.35}CoO_2 1.4D_2O$.

LIST OF REFERENCES

[1] Takada, K., H. Sakurai, E. Takayama-Muromachi, F. Izumi, R. A. Dilanian and T. Sasaki, "Superconductivity in two dimensional CoO_2 layers", *Nature* **422**, 53 (2003).

[2] R. Jin, B. C. Sales, P. Khalifah, and D. Mandrus, "Observation of Bulk Superconductivity in $Na_xCoO_2yH_2O$ and $Na_xCoO_2yD_2O$ Powder and Single Crystals", *Phys. Rev. Lett.*, **91**, 217001 (2003).

[3] R. E. Schaak, T. Klimczuk, M. L. Foo and R. J. Cava, "Superconductivity phase diagram of Na_xCoO_2-1.3H_2O", *Nature* **424**, 527 (2003).

[4] J. W. Lynn, Q. Huang, C. M. Brown, V. L. Miller, M. L. Foo, R. E. Schaak, C. Y. Jones, E. A. Mackey and R.J. Cava, "Structure and dynamics of superconducting Na_xCoO_2 hydrate and its unhydrated analog", *Phys. Rev. B* **68**, 214516 (2003).

[5] J. D. Jorgensen, M. Avdeev, D. G. Hinks, J. C. Burley and S. Short, "Crystal structure of the sodium cobaltate deuterated superconductor $Na_xCoO_2$4xD_2O (x~1/3)", *Phys. Rev. B* **68**, 214517 (2003).

[6] H. K. Onnes, *Communications from the Physical Laboratory of the University of Leiden* (1911).

[7] W. Meissner and R. Ochsenfeld, "Ein neuer Effekt bei Eintritt der Supraleitfahigkeit" *Naturwissenschaften* **21**, 787–788 (1933).

[8] J. Bardeen, L. N. Cooper, and J. R. Schrieffer, "Theory of Superconductivity" *Physical Review* **108**, 1175–1204 (1957).

[9] E. Maxwell, "Isotope Effect in the Superconductivity of Mercury", *Physical Review* **78**, 477 (1950).

[10] C. A. Reynolds, B. Serin, W. H. Wright, and L. B. Nesbit, "Superconductivity of Isotopes of Mercury", *Physical Review* **78**, 487 (1950).

[11] W. S. Corak, B. B. Goodman, C. B. Satterthwaite, and A.Wexler, "Exponential Temperature Dependence of the Electronic Specific Heat of Superconducting Vanadium", *Physical Review* **96**, 1442 (1954).

[12] W. S. Corak, B. B. Goodman, C. B. Satterthwaite, and A.Wexler, "Atomic Heats of Normal and Superconducting Vanadium", *Physical Review* **102**, 656 (1956).

[13] G. Bednorz, and K. A. Müller, "Possible high *Tc* superconductivity in the Ba-La-Cu-O system", *Z. Phys. B* **64**, 189–193 (1986).

[14] M. K. Wu "Superconductivity at 93 K in a New Mixed-Phase Y-Ba-Cu-O Compound System at Ambient Pressure", *Physical Review Letters* **58**, 908 (1987).

[15] D. A. Wollman, D. J. V. Harlingen, W. C. Lee, D. M. Ginsberg, and A. J. Leggett, "Experimental determination of the superconducting pairing state in YBCO from the phase coherence of YBCO-Pb dc SQUIDs", *Physical Review Letters* **71**, 2134–2137 (1993).

[16] C. C. Tsuei, J. R. Kirtley, C. C. Chi, L. S. Yu-Jahnes, A. Gupta, T. Shaw, J. Z. Sun, and M. B. Ketchen "Pairing Symmetry and Flux Quantization in a Tricrystal Superconducting Ring of YBa2Cu3O7−δ", *Physical Review Letters* **73**, 593–596 (1994).

[17] C. E. Gough, M. S. Colclough, E. M. Forgan, R. G. Jordan, M. Keene, C. M. Muirhead, A. I. M. Rae, N. Thomas, J. S. Abell, and S. Sutton, "Flux quantization in a high-Tc superconductor", *Nature* **326**, 855 (1987).

[18] A. Lanzara, P. V. Bogdanov, X. J. Zhou, S. A. Kellar, D. L. Feng, E. D. Lu, T. Yoshida, H. Eisaki, A. Fujimori, K. Kishios, J.-I. Shimoyama, T. Noda, S. Uchida, Z. Hussain, and Z.-X. Shen, "Evidence for ubiquitous strong electronphonon coupling in high-temperature superconductors", *Nature* **412**, 510–514 (2001).

[19] S.W. Lovesey, "Theory of neutron scattering from condensed matter", Oxford University Press.

[20] "Neutron Scattering", *Los Alamos Science **19*** (1990), LANL publications.

[21] G.L. Squires, "Introduction to the Theory of Thermal Neutron Scattering" Dover Publications.

[22] G. Shirane, S. M. Shapiro, and J. M. Tranquada, "Neutron Scattering with a Triple-Axis Spectrometer : Basic Techniques", Cambridge University Press.

[23] C.-K Loong, S. Ikeda, and J. M. Carpenter, *Nucl. Instrum. Meth. Phys. Res.* **A260**, 381 (1987).

[24] T. Egami, S. J. L. Billinge, "Underneath the Bragg-Peaks: Structural Analysis of Complex Materials", Elsevier, New York (2003).

[25] T. Proffen, S. J. L. Billinge, T. Egami, and D. Louca, "Structural analysis of complex materials using the atomic pair distribution function-A practical guide", *Z. Kristallogr., **218***, 132– 143 (2003).

[26] T. Proffen, T. Egami, S. J. L. Billinge, A. K. Cheetham, D. Louca, and J. B. Parise, "Building a high resolution total scattering powder diffractometer-Upgrade of NPD at MLNSC", *Appl. Phys. A*, **74**, S163– S165 (2002).

[27] P. F Peterson, M. Gutmann, T. Proffen, and S. J. L. Billinge, "PDFgetN: A user-friendly program to extract the total scattering structure function and the pair distribution function from neutron powder diffraction data" *J. Appl. Crystallogr., **33***, 1192 (2000).

[28] T. Proffen, and S. J. L. Billinge, "PDFFIT, a program for full profile structural refinement of the atomic pair distribution function", *J. Appl. Crystallogr., **32***, 572– 575 (1999).

[29] Y. Ono, R. Ishikawa, Y. Miyazaki, Y. Ishii, Y. Morii and T. Kajitani, "Crystal Structure, Electric and Magnetic Properties of β-Na_xCoO_2"*, J. Solid State Chem*., **166**, 177 (2002).

[30] B.H. Toby, and T. Egami, "Accuracy of Pair Distribution Function Analysis Applied to Crystalline and Non-Crystalline Materials", *Acta Cryst. A* **48** 336–346 (1992).

[31] M.L. Foo, Y.Y. Wang, S. Watauchi, H.W. Zandbergen, T. He, R.J.Cava, and N.P Ong, "Charge Ordering, Commensurability, and Metallicity in the Phase Diagram of the Layered Na_xCoO_2", *Phys. Rev. Lett*. **92,** 247001 (2004).

[32] C. J. Milne, D. N. Argyriou, A. Chemseddine, N. Aliouane, J. Veira, S. Landsgesell, and D. Alber, "Revised superconducting phase diagram of hole doped Nax(H3O)zCoO2yH2O", *Phys. Rev. Lett.* **93**, 247007 (2004).

[33] Y. Krockenberger, I. Fritsch, G. Christiani, H.-U. Habermeier, Li Yu, C. Bernhard, and B. Keimer, L. Alff, "Superconductivity in epitaxial thin films of $Na_xCoO_2{\cdot}yD_2O$", *Appl. Phys. Lett.* **88**, 162501 (2006).

[34] Yayu Wang, Nyrissa S. Rogado, R. J. Cava, and N. P. Ong, "Spin entropy as the likely source of enhanced thermopower in NaxCo2O4", *Nature* **423**, 425 (2003).

[35] P. W. Barnes, M. Avdeev, J. D. Jorgensen, D. G. Hinks, H. Claus, and S. Short "Superconductivity and cobalt oxidation state in metastable $Na_xCoO_{2-\delta}{\cdot}yH_2O$ (x~1/3;y~4x)", *Phys Rev. B* **72**, 134515 (2005).

[36] D. Eisenberg, and W. Kauzmann, "Structure and properties of water", Oxford University press (1969).

[37] F. Franks, "Water: A Matrix of Life", 2nd Ed., Royal Society of chemistry,Cambridge, UK (2000).

[38] L. Pauling, "General Chemistry", Dover Publications (1991).

[39] K. Ichikawa, Y. Kameda, T. Yamaguchi, H. Wakita and M. Misawa, "Neutron-diffraction investigation of the intramolecular structure of a water molecule in the liquid-phase at high-temperatures", *Mol. Phys.* **73**, 79-86 (1991).

[40] J. B. Hasted, "Water A comprehensive treatise", Vol 1, Ed. F. Franks (Plenum Press, New York, 1972).

[41] P. L. Silvestrelli and M. Parrinello, "Structural, electronic, and bonding properties of liquid water from first principles", *J. Chem. Phys.*, **111**, 3572-3580 (1999).

[42] E. Espinosa, E. Molins, C. Lecomte, "Hydrogen bond strengths revealed by topological analyses of experimentally observed electron densities", *Chem. Phys. Lett.* **285**, 170-173(1998).

[43] V. F Petrenko, and R. W. Whitworth, "The Physics of ice", Oxford University Press (1999).

[44] N. H. Fletcher, "The Chemical Physics of Ice", Cambridge University Press (1971).

[45] K. Takada, H. Sakurai, E. Takayama-Muromachi, F.Izumi, R.A. Dilanian and T. Sasaki, "Superconductivity in two-dimensional CoO2 layers", *Nature* **422** 53 (2003).

[46] J. M. Hermida-Ramón and G.Karlström "Study of the hydronium ion in water, A combined quantum chemical and statistical mechanical treatment", *J. Mol. Struct. Theochem* **712** (2004) 167-173.

[47] A. I. Kolesnikov, J.-C. Li, D. K. Ross, V. V. Sinitzin, O. I. Barkalov, E. L. Bokhenkov and E. G. Ponyatovskii, "Inelastic incoherent neutron scattering study of D_2O and H_2O ice VIII in the range 2-140 meV", *Phys. Lett. A*, **168**, 308 (1992).

[48] K. Toukan, M. A. Ricci, S.-H. Chen, C.-K. Loong, D. L. Price and J. Teixeira, "Neutron-scattering measurements of wave-vector-dependent hydrogen density of states in liquid water", *Phys. Rev. A,* **37**, 2580 (1988).

[49] Morrison, I., and S. Jenkins, "First Principles Lattice Dynamics Studies of the Vibrational Spectra of Ice", *Physica B,* **263-264**, 442 (1999).

[50] J. D. Jorgensen, M. Avdeev, D. G. Hinks, P. W. Barnes, and S. Short "Thermal Expansion and Compressibility in Superconducting NaxCoO2.4xD2O (x≈1/3): Evidence for Pressure-Induced Charge Redistribution", *Phys. Rev. B* **72**, 224515 (2005).

[51] M.J. Iedema, A.A. Tsekouras, M. Dresser, J. Brad Rowland, D. Doering, J.P. Cowin "Ferroelectric Water Ice", *J. Phys. Chem*. **102**, 9203(1998).

[52] Xingcai Su, L. Lianos, Y. Ron Shen, and Gabor A. Somorjai **"**Surface-Induced Ferroelectric Ice on Pt(111)", *Phys. Rev. Lett.* **80**, 1533–1536 (1998).

[53] Sherwin J. Singer, Jer-Lai Kuo, Tomas K. Hirsch, Chris Knight, Lars Ojamäe, and Michael L. Klein "Hydrogen-Bond Topology and the Ice VII/VIII and Ice I*h*/XI Proton-Ordering Phase Transitions", *Phys. Rev. Lett.* **94**, 135701 (2005).

[54] G. P Johari, and E. Whalley "The dielectric properties of ice Ih in the range 272-133K", *J Chem Phys* **75**, 1333 (1981).

VITA

Cinzia Metallo was born in Rome, Italy. In 2003, she graduated from the University of Rome with a M.S. (Laurea) in Biophysics. From Rome she went to the University of Tennessee, Knoxville, where she was awarded the Tennessee Advanced Materials Laboratory (TAML) scholarship. In 2006, she received a second M.S. in Physics with a concentration in solid state physics. She is a member of the Sigma Pi Sigma National Physics Honor Society and she is coauthor of several scientific publications. Her past research activities include the synthesis of polycrystalline samples by solid state reaction, surface resistivity measurements, neutron and X-ray diffraction experiments on a variety of materials, and the pair density function (PDF) technique.